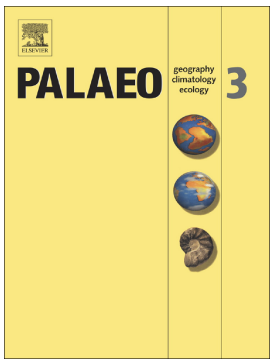

Paired isotope records of carbonate and organic matter from the Middle Ordovician of Argentina: Intrabasinal variation and effects of the marine chemocline

Miles A. Henderson, Fernanda Serra, Nicolás A. Feltes, Guillermo L. Albanesi, Linda C. Kah

PII: S0031-0182(17)30923-9
DOI: doi:10.1016/j.palaeo.2017.10.018
Reference: PALAEO 8485

To appear in: *Palaeogeography, Palaeoclimatology, Palaeoecology*

Received date: 5 September 2017
Revised date: 17 October 2017
Accepted date: 17 October 2017

Please cite this article as: Miles A. Henderson, Fernanda Serra, Nicolás A. Feltes, Guillermo L. Albanesi, Linda C. Kah , Paired isotope records of carbonate and organic matter from the Middle Ordovician of Argentina: Intrabasinal variation and effects of the marine chemocline. The address for the corresponding author was captured as affiliation for all authors. Please check if appropriate. Palaeo(2017), doi:10.1016/j.palaeo.2017.10.018

Paired isotope records of carbonate and organic matter from the Middle Ordovician of Argentina: Intrabasinal variation and effects of the marine chemocline

Miles A. Henderson [a]*, Fernanda Serra [b], Nicolás A. Feltes [bc], Guillermo L. Albanesi [bc], and Linda C. Kah [a]

[a] *Department of Earth and Planetary Sciences, University of Tennessee, Knoxville, TN 37996 United States*

[b] *CICTERRA (CONICET-UNC), Av. Vélez Sarsfield 1611, Córdoba X5016GCA, Argentina*

[c] *CONICET, Museo de Paleontolía, CIGEA, FCEFyN, Av. Vélez Sarsfield 299, Córdoba, X5000FCO, Argentina*

*milesh@utk.edu

Abstract

We investigate the expression of the Middle Darriwilian isotope carbon excursion (MDICE) across marine shelf environments in the Argentine Precordillera. Previous work identified the MDICE in the Las Chacritas Formation in Argentina, but did not recognize the expression of the MDICE in time-equivalent strata of the deeper-water Las Aguaditas Formation (Albanesi et al., 2013; Palaeogeography, Palaeoclimatology, Palaeoecology, v. 398, p. 48–66). Recent biostratigraphic investigations of these units have, for the first time, provided the opportunity for high-resolution correlation, which suggest that the MDICE, or at least the initiation of the MDICE, should be observed in both the Las Chacritas and Las Aguaditas formations. Here we present new paired carbon isotope data of carbonate and organic carbon from the Las Chacritas and Las Aguaditas formations. We identify a 2 ‰ positive shift in the

isotopic composition of marine carbonate in the Las Chacritas Formation, whereas values abruptly fall to < −1 ‰ in equivalent strata of the Las Aguaditas Formation. This is the first record of divergence from the globally recognized MDICE event. There are also small, yet distinct differences in the isotopic composition of marine organic matter between these two sections. We suggest that the divergent C-isotope trends of carbonate in the Las Chacritas and Las Aguaditas formations represent deposition in fundamentally different parts of the water column — above and below the marine chemocline, respectively — during the MDICE interval. This interpretation is consistent with data from the Las Aguaditas Formation that shows elevated Mn and Fe concentrations in carbonate phases with little evidence for recrystallization, and with a growing consensus for regionally anoxic conditions for the Middle Ordovician. Our data indicate that redox gradients can play a critical role in the behavior of marine carbon isotope excursions.

Keywords: Carbon isotopes; Chemostratigraphy; MDICE; Precordillera; Darriwilian

1. Introduction

The carbon isotope record of marine carbonate minerals has become a widely used geochemical tool for correlating stratigraphic sections (cf. Berger and Vincent, 1981; Saltzman and Thomas, 2012; Kah et al., 2012; Azmy et al., 2014). Because dissolved inorganic carbon (DIC) in surface oceans has a relatively short residence time relative to oceanic mixing, high resolution stratigraphic signatures may be resolved. Globally recognized excursions in the carbon isotope composition of marine carbonate minerals thus allow for chemostratigraphic correlation among geographically disparate sections, even in the absence of biostratigraphic control (Halverson et al., 2005).

Marine carbonate rocks of the Ordovician are bracketed by large (+5 ‰ to +7 ‰) perturbations in the isotopic composition of marine DIC including the late Cambrian Steptoean positive carbon isotope excursion (SPICE; Saltzman et al., 1998) and the late Ordovician Katian (Saltzman and Young, 2005) and Hirnantian carbon isotope excursions (HICE; Brenchley et al., 1994; Finney et al., 1999). These large-scale perturbations have been associated with episodes of climatic cooling, enhanced ocean circulation, and elevated organic productivity (Saltzman, 2005). Between these periods of isotopic volatility, stability in marine carbon isotopes is hypothesized to result from generally sluggish circulation and reduced organic productivity driven by greenhouse climates. Such periods of enhanced stability are recognized by only small-magnitude isotope excursions (to approximately +2 ‰), such as the Middle Darriwilian isotope carbon excursion (MDICE).

The MDICE was first recognized in Baltoscandia (Ainsaar et al., 2004; Meidla et al., 2004; Martma, 2005; Ainsaar et al., 2007; Kaljo et al., 2007; Calner et al., 2014), and later recognized in equivalent-aged strata in China (Schmitz et al., 2010; Zhang et al., 2010; Kah et

al., 2016), North America (Leslie et al., 2011; Thompson et al., 2012; Young et al., 2016), and in the Precordillera of Argentina (Thompson et al., 2012; Albanesi et al., 2013), making it one of the most widely recognized Ordovician excursions. The MDICE is characterized by a near monotonic rise of carbon isotope compositions from approximately −2 ‰ during the Dapingian to values > +1 ‰ during the middle Darriwilian. Although relatively small in magnitude, the MDICE broadly coincides in time with an inferred decrease in ocean temperatures prior to the Hirnantian glaciation (Trotter et al., 2008) and potential deep-water ventilation (Thompson et al., 2012; Marenco et al., 2013; Kah et al., 2016), both of which suggest that fundamental changes in the behavior of the oceans may have participated in the Great Ordovician Biodiversification Event (GOBE; Webby et al., 2004; Harper et al., 2006; Servais et al., 2010; Rasmussen et al., 2016). The behavior of the MDICE across a variety of environments may therefore provide an additional constraint on the physical and chemical behavior of marine systems at this time.

Recent revisions to the biostratigraphy of Darriwilian carbonate successions in the Argentine Precordillera (Serra et al., 2015; Feltes et al., 2016) suggest that the MDICE, or at least its initiation, should occur in the upper *Eoplacognathus pseudoplanus* and lower *Eoplacognathus suecicus* conodont biozones of the Las Chacritas and Las Aguaditas formations, whose facies represent distinct environments on a deepening marine shelf. Here we use recent biostratigraphic correlations to explore the relationships between C-isotope records of carbonate and organic matter during the middle Darriwilian within time-equivalent, yet distinct, depositional environments. This is the first study to use paired C-isotopes record of carbonate and organic carbon to evaluate the expression of the MDICE across time correlative units and distinct depositional environments, and will further our understanding of potential marine conditions at this critical interval in Earth history.

2. Geologic setting and age

2.1 The Argentine Precordillera

The Precordillera is the remnant of an independent microcontinent terrane that rifted from the southeast margin of Laurentia in the early Cambrian (ca. 530–539 Ma; Thomas et al., 2001), and migrated across the Iapetus ocean before docking with Gondwana during the Late Ordovician (Ramos et al., 1986; Astini et al., 1995; Thomas and Astini, 1996; Astini and Thomas, 1999; Thomas et al., 2002; Thomas, 2011). Although the paleogeographic location of the Precordillera through this interval is not well constrained (Fig. 1; Cocks and Torsvik, 2002); migration of the Precordilleran microcontinent across the Iapetus Ocean is inferred from a decrease in fauna with Laurentian affinity through the Tremadocian and an increase in biotic exchange with Baltica and Gondwana during the Darriwilian and Sandbian (Harper et al., 1996; Benedetto, 2004; Benedetto et al., 2009). Proximity of the Precordillera terrane to the Gondwanan margin by the Dapingian (Thompson et al., 2012) is confirmed by the presence of bentonite deposits that are associated with volcanism in the Famatina arc province (Astini et al., 1995; Huff et al., 1995; Huff et al., 1997; Huff et al., 1998; Pankhurst et al., 2000; Fanning et al., 2004).

Within the Precordillera, more than 2500 m of Cambrian to Ordovician strata are exposed in a series of North–South trending thrust sheets that comprise the Andean foothills between 28˚ and 33˚ S (Fig. 2; Ramos et al., 1986; Astini et al., 1995; Keller, 1999). The region is subdivided into the eastern and western tectofacies, which record carbonate, evaporite, and siliciclastic deposition in marine shelf and slope environments (Astini et al., 1995). Little deformed and unmetamorphosed strata of the eastern tectofacies record a transition from passive margin

carbonate deposition to siliciclastic deposition associated with the development of a foreland basin inboard of the Precordillera terrane (Astini et al., 1995). Deeper-water facies of the western tectofacies are more strongly deformed, and were subjected to low-grade metamorphism during regional shortening (Allmendinger et al., 1990; Zapata and Allmendinger, 1996; Alvarez-Marron et al., 2006; Allmendinger and Judge, 2014).

2.2. Middle Ordovician strata

Relatively undeformed Early and Middle Ordovician strata are exposed within the Niquivil thrust sheet in San Juan Province, Argentina (von Gosen, 1997). Strata include the Tremadocian La Silla Formation, the Floian–Darriwilian San Juan Formation, and the Darriwilian–Sandbian Las Chacritas, Las Aguaditas, and Gualcamayo formations. The transition to Middle Ordovician (Dapingian) strata occurs in the San Juan Formation, which records the transition from shallow subtidal carbonate deposition to storm-dominated subtidal deposits (Cañas, 2003). The contact between the San Juan Formation and overlying strata of the Las Chacritas, Las Aguaditas, and Gualcamayo formations is marked by a transition to deeper-water, siliciclastic-rich to siliciclastic-dominated facies (Astini, 1995b; Carrera and Astini, 1998). This transition is time-transgressive (Astini, 1995a), reflecting differential subsidence as the Precordilleran terrane converged upon Gondwana. In some places (e.g., Talacasto and Pachaco sections, Thompson et al., 2012), the San Juan Formation is terminated by an unconformity and overlain by Silurian strata. This unconformity is associated with the formation of the Talacasto-Tambolar Arch and migration of the forebulge during the Late Ordovician, and resulted in the removal of late Darriwilian through early Silurian strata across much of the Precordillera (Astini et al., 1995).

Precise chronologic ages are best determined for the San Juan Formation, which contains abundant bentonites (Huff et al., 1995). The most recent determination of dates from the San Juan Formation range from 473.45 ± 0.70 Ma to 469.53 ± 0.62 Ma ($U\text{-}Pb_{zircon}$; Thompson et al., 2012), which is consistent with earlier analyses that yielded dates of 470 ± 3.3 Ma to 469 ± 3.2 Ma (Fanning et al., 2004). As noted previously, the upper San Juan Formation is diachronous and, in places, is truncated by an unconformity. These Dapingian ages therefore do not distinctly define the age of the uppermost San Juan Formation. There are no current geochronological dates to precisely constrain the age of overlying Las Chacritas, Las Aguaditas, and Gualcamayo formations.

2.2.1. Las Chacritas Formation

For this study, the Las Chacritas Formation was investigated in the northern La Trampa Range along the Las Chacritas River, approximately 37 km south of San Jose de Jáchal, San Juan Province, Argentina (30°33'39.06" S, 68°51'49.62" W; Fig. 2). Sedimentologic and biostratigraphic relationships at the Las Chacritas River section have been previously reported (Peralta and Baldis, 1995; Carrera and Astini, 1998; Peralta et al., 1999; Heredia et al., 2005; Albanesi et al., 2013; Serra et al., 2015; Serra et al., 2017). The following is a summary of both previous investigations and current observations of the Las Chacritas River section. The Las Chacritas Formation is an approximately 60-m-thick succession of interbedded carbonate and black shale that conformably, and transitionally, overlies fossiliferous packstone, wackestone, and mudstone lithologies of the San Juan Formation (Keller, 1999). Strata of San Juan Formation vary from 5 cm to 1 m in thickness, thinning toward the top of the unit. The contact between the

San Juan Formation and the overlying Las Chacritas Formation is marked by a hardground surface and the occurrence of a thin bentonite horizon.

The Las Chacritas Formation is divided into two members; a lower member of fossiliferous mudstone, wackestone, and packstone and an upper member of mudstone and spiculitic mudstone, with a thin interval of bioclastic grainstone (Peralta et al., 1999). At the locality sampled for this study, the Las Chacritas Formation is approximately 65 m thick based on field measurement combined with conodont biostratigraphy (Serra et al., 2015). The formation consists of 2–10 cm thick beds of fossiliferous mudstone, wackestone, and packstone interbedded with < 2 cm thick partings of black shale. Higher in the section, fossiliferous wackestone and spiculitic mudstone beds are thinner (2–5 cm thick) with correspondingly thicker (> 2 cm thick) interbeds of black shale. Carrera (1997) identified sponges in the Las Chacritas Formation belonging to the *Archaeoscyphia* Biofacies which is associated with deposition below fair-weather wave base, but above storm wave base. The top of the Las Chacritas Formation is marked by a regional unconformity overlain by Sandbian calcareous and siliciclastic deposits of the deeper-water, middle member of the Las Aguaditas Formation (Peralta et al., 1999).

2.2.2. Las Aguaditas Formation

The Las Aguaditas Formation was investigated at its type section along Las Aguaditas Creek in the Los Blanquitos Range, approximately 10 km to the southwest of San Jose de Jáchal, San Juan Province, Argentina (30°18'16.38" S, 68°49'13.40" W; Fig. 2). The following is a summary of previous (Keller et al., 1993; Astini, 1995b; Keller, 1999; Albanesi et al., 2013; Feltes et al., 2016) and current observations of the Las Aguaditas Formation. At Las Aguaditas Creek, the Las Aguaditas Formation conformably, and gradationally, overlies fossiliferous and

nodular packstone, wackestone, and mudstone lithologies of the San Juan Formation (Keller et al., 1993). Transitional strata of the upper San Juan Formation are dominated by 5–10-cm thick mudstone beds, although a 20-cm-thick packstone interval was observed just below the contact with calcareous mudstone of the overlying Las Aguaditas Formation.

The Las Aguaditas Formation is approximately 300 m thick, and spans Darriwilian through the early Sandbian time (Keller et al., 1993; Astini, 1995b; Feltes, 2017). Darriwilian-age strata occur in the 43-meter-thick lower member, which is composed of thinly bedded (1–5 cm) carbonate mudstone and wackestone, interbedded with prominent intervals (< 10 cm thick) of calcareous black shale. Limestone of the Las Aguaditas Formation contains abundant sponge spicules and trilobite fragments, yet lacks evidence of bioturbation. Nodular wackestone intervals exhibit differential cementation and dissolution associated with bioturbation on the seafloor (Keller et al., 1993). The interpreted depositional setting for the lower member of the Las Aguaditas Formation is in relatively deep water, at or below storm wave base. The top of the lower member of the Las Aguaditas Formation is marked by a disconformity identified by the abrupt appearance of Sandbian conodonts (Albanesi et al., 2013; Feltes et al., 2016).

2.3. Biostratigraphic correlation of the Las Chacritas and Las Aguaditas formations

A general chronologic framework of Ordovician strata in the Precordillera, based on conodont and graptolite biostratigraphy, is well established (Albanesi and Ortega, 2016). High-resolution conodont and graptolite biostratigraphic investigations are consistent with a primarily Darriwilian age for the Las Chacritas and Las Aguaditas formations, and have provided a more detailed correlation between these two units (Figs. 3 and 4; Albanesi et al., 2013; Serra et al., 2015; Feltes et al., 2016; Serra et al., 2017). Conodont elements are abundant in the upper San

Juan and Las Chacritas formations (Serra et al., 2015). In deeper water facies of the lower member of the Las Aguaditas Formation, relatively few conodont elements were recovered (Feltes et al., 2016). Conodont fauna of the Precordillera are generally dominated by tropical, generally shallow-water (< 200 m) assemblages in the Early Ordovician, with an increasing number of temperate water taxa identified in the Middle Ordovician (Albanesi and Ortega, 2016).

Conodont elements recovered from limestone of the Las Chacritas and Las Aguaditas formations record the presence of *Yangtzeplacognathus crassus*, *E. pseudoplanus*, *E. suecicus*, and *Pygodus anserinus* Zones, with the *Lenodus variabilis* and *Y. crassus* Zones occurring in the uppermost San Juan Formation (Fig. 3). Using the chronostratigraphic correlations of Bergström et al. (2009) and Webby et al. (2004), lower Darriwilian conodont Zones (stage slice (SS) Dw1 of Bergström et al., 2009 and time slice (TS) 4a of Webby et al., 2004) are identified in the *L. variabilis* Zone and correlate to the *L. variabilis* Zone identified in Scandinavia and China, and the *Histiodella sinuosa* Zone in North America (Albanesi and Ortega, 2016). In the sections investigated for this study, the top of the *L. variabilis* Zone was identified in the San Juan Formation, 3.75 m below the base of the Las Chacritas Formation and 24 m below the base of the Las Aguaditas Formation.

The *Y. crassus* Zone, which marks the transition to the Middle Darriwilian (SS Dw2, TS 4b) is approximately 40 m thick in the Las Chacritas Formation and 36 m thick in the Las Aguaditas Formation. The lower boundary of the *Y. crassus* Zone is marked by the presence of the *Paroistodus horridus* subzone in the Precordillera (Albanesi and Barnes, 2000). The upper boundary of the *Y. crassus* Zone is marked by the presence of *Dzikodus tablepointensis* in the Las Aguaditas Formation and the first appearance of *Eoplacognathus pseudoplanus* in the Las

Chacritas Formation (Albanesi and Barnes, 2000; Albanesi et al., 2013; Serra et al., 2015; Feltes et al., 2016). The *Y. crassus* Zone correlates to strata in south China, Scandinavia, Baltica, and the North Atlantic (Fig. 3; cf. Serra et al., 2015).

The base of the *E. pseudoplanus* Zone (SS Dw2) is identified 36 m above the base of the Las Chacritas Formation and extends to 58 m above the base of the unit (Serra et al., 2015). In the Las Aguaditas Formation, the *E. pseudoplanus* Zone is 24 m thick and characterized by the co-occurrence of *D. tablepointensis*. The *E. pseudoplanus* Zone is identified in shallow water environments in Baltoscandia, whereas *D. tablepointensis* is characteristic of deeper-water water environments found in China and Newfoundland (Feltes et al., 2016). The upper *E. pseudoplanus* Zone in the Precordillera is marked by the occurrence of *Microzarkodina hagetiana* and *M. ozarkodella* (Serra et al., 2015; Feltes et al., 2016). The *E. pseudoplanus* Zone is equivalent to the *E. pseudoplanus* Zone in Baltoscandia. Identification of the *Histiodella holodenta* subzone in the top of the *E. pseudoplanus* Zone allows for correlation to China (Zhang, 1998), Baltoscandia (Viira, 2011), and the uppermost Table Point Formation in the Table Head Group of Newfoundland (Stouge, 1984). In the Las Chacritas River section, the top of the *E. pseudoplanus* Zone is marked by the occurrence of *Histiodella kristinae* which typifies the lower subzone of the *E. suecicus* Zone and defines the rest of SS Dw2 in the Precordillera (Serra et al., 2015). The *E. suecicus* zone correlates to the *E. suecicus* Zone of Baltoscandia and with the *H. kristinae* Zone and the *Periodon zgierzensis* Zone of the Table Point Group of Western Newfoundland (Stouge, 2012; Serra et al., 2015).

A disconformity is identified at the top of both the Las Chacritas and Las Aguaditas formations by the occurrence of the Sandbian conodont elements of *Pygodus anserinus* (SS Sa1; Albanesi et al., 2013; Serra et al., 2015; Feltes et al., 2016). In the Las Chacritas Formation, the

top of the *E. suecicus* (SS Dw2, TS 4b) and the *P. serra* (SS Dw3, TS 4C) conodont zones are missing. In the deeper water Las Aguaditas Formation, the top of the *E. pseudoplanus,* the *E. suecicus,* the *P. serra,* and lower subzone of the *P. anserinus* zones have been removed. More extensive removal of deeper water strata from the Las Aguaditas Formation cannot readily be explained by sea level fall, and has thus been attributed to forebulge migration. Emplacement of a tectonic load on a rigid lithosphere typically results in migration of the forebulge away from the tectonic load, resulting in preferential uplift and erosion of shallower water environments (Beaumont, 1981). Patterns of missing time in the Precordillera are attributed to forebuldge migration associated with oblique convergence of the northward-deepening carbonate platform with the Gondwanan margin that resulted in flexural uplift and differential erosion of initially deeper water environments (cf. Astini et al., 1995).

3. Analytical methods

3.1. Petrographic screening

Carbonate samples were cut into mirror-image billets used, respectively, for thin sections and polished thick sections. Thin and thick sections were analyzed using conventional petrographic and cathodoluminescence (CL) analysis to assess the range of carbonate fabrics and identify phases that show evidence of post-depositional recrystallization. Discrete carbonate phases were drilled from polished thick sections with 0.3 or 0.5 mm drill bits using a Servo tabletop drill press. Splits of resulting powders were used for isotopic and elemental analyses.

3.2. Isotopic analyses of carbonate phases

For isotopic analysis of carbonate phases, approximately 0.25 mg of carbonate powder was loaded into a glass vial with a septum cap, flushed with ultra-high purity helium gas for 5 minutes, then acidified with 100 µl of phosphoric acid at 72˚C for at least 1 hour. The resulting CO_2 gas was sampled using a Thermo-Finnegan GasBench II and transferred into a Thermo-Finnegan DeltaPlus XL mass spectrometer for isotope ratio measurement at the University of Tennessee. Isotope ratios of carbon and oxygen are reported in delta notation as per mil (‰) relative to the Vienna Pee Dee Belemnite (VPDB) standard. Precision and calibration of data were monitored through routine analysis of internal laboratory and the IAEA LSVEC ($\delta^{13}C$ = −46.6 ‰; $\delta^{18}O$ = −26.41 ‰) and NBS 19 ($\delta^{13}C$ = +1.95 ‰; $\delta^{18}O$ = −2.2 ‰) international standards. Analyses were reproducible to better than ± 0.1 ‰ for carbon and ± 0.2 ‰ for oxygen, based on analysis of replicates and internal laboratory standards.

3.3. Elemental analyses

Drilled carbonate powders were analyzed for major (Ca, Mg) and trace (Sr, Mn, Fe) element concentrations with a Perkin-Elmer Optima 2100 DV inductively coupled plasma optical emission spectrometer (ICP-OES) at the University of Tennessee. Approximately 1 mg of carbonate powder was acidified with trace metal grade 2 % HNO_3, and agitated for > 1 hour to assure complete dissolution of carbonate. Solutions were centrifuged and decanted into a clean sample tubes to remove any insoluble materials prior to analysis. Spectra were calibrated using a series of gravimetric standards, with reproducibility for all elements better than ± 5 % based on replicate measurements of sample and standard solutions.

3.4. Isotopic analyses of organic matter

For isotope determination of organic carbon phases, approximately 100 mg of bulk sample powder was acidified with 10 ml of 3M HCl until all reaction was complete. Residual powders were rinsed three times with Milli-Q water and dried at 50˚C. Approximately 3.5 mg of insoluble residue was weighed into tin cups for combustion in a Costech ECS 4010 elemental analyzer. The resulting CO_2 gas was transferred into a Thermo-Finnegan DeltaPlus XL mass spectrometer via a Thermo-Finnegan Conflo III interface at the University of Tennessee. Precision and calibration of data were monitored through routine analysis of internal laboratory and the USGS40 and USGS41 ($\delta^{13}C$ equal to −26.39 and +37.63 ‰, respectively) international standards. Isotope ratios are reported in delta notation as per mil (‰) relative to the Vienna Pee Dee Belemnite (VPDB) standard. Analyses were reproducible to better than ± 0.12 ‰ based on analysis of replicates and internal laboratory standards.

4. Results and interpretation

4.1. Petrographic characterization

Petrographic analysis of Darriwilian carbonate rocks from the San Juan and overlying Las Chacritas and Las Aguaditas formations are consistent with field observations that strata are composed of primarily carbonate mudstone, wackestone, and packstone. Petrographic observations, however, provide additional detail that highlights the similarities and differences between the formations. Strata of the upper San Juan Formation in both the Las Chacritas River and Las Aguaditas Creek sections are composed of fossiliferous wackestone and packstone (Figs. 5A and 6A), dominated by a matrix of either micrite or finely crystalline microspar (< 5 μm). Dolomitization is rare in all formations and, when present, is found in sections that have also experienced fabric destructive recrystallization of micrite to sparry calcite cement.

Stylolitization is common in the upper San Juan Formation and the Las Chacritas Formation, but is not easily defined in shale-rich deposits of the Las Aguaditas Formation. Skeletal grains are common in the San Juan Formation and consist of bryozoans, gastropods, echinoderms, brachiopods, and sponge spicules. Skeletal grains in the San Juan Formation are typically 0.02 to 1.6 mm in size, with measurements representing the longest diameter of a circumscribed ellipse; most skeletal fragments represent disarticulated elements, yet with few broken elements. Preservation of skeletal microfabrics is variable, with most echinoderm, brachiopod, and trilobite elements retaining their primary microstructures; by contrast, gastropods and sponges are more commonly represented by molds filled with fine calcite spar.

Deepening in the Precordillera is reflected in the transition from subtidal packstone of the upper San Juan Formation to predominantly wackestone and carbonate mudstone in the Las Chacritas and Las Aguaditas formations. The Las Chacritas Formation is composed largely of carbonate mudstone (Fig. 5B) and wackestone, with intermittent packstone intervals (Fig. 5C) in the *E. pseudoplanus* Zone. Carbonate mudstone in the Las Chacritas Formation is typically poorly laminated, and contains continuous to discontinuous clay laminations, which occur primarily as drapes along bedding planes. In some sections, micrite has been recrystallized to finely crystalline (< 5 μm) microspar. Allochems in the Las Chacritas Formation consist of micritic intraclasts (Fig. 5B), brachiopod and trilobite fragments, and sponge spicules. Skeletal microfabrics are variably preserved, with brachiopod and sponge spicules largely recrystallized and the prismatic microstructure of trilobite fragments nearly always preserved. Fewer skeletal grains are observed toward the top of the Las Chacritas Formation, where only rare trilobite fragments and recrystallized sponge spicules are identified. Recrystallization of matrix components to a coarse calcite spar is observed, although recrystallization is not abundant and is

concentrated within rare, more fossiliferous horizons. Disseminated pyrite is also identified throughout the Las Chacritas Formation (Figs. 5B–D) and does not appear to be associated with any specific depositional texture.

The Las Aguaditas Formation is composed primarily of carbonate mudstone and wackestone with intermittent clay and silt laminations. Clay minerals are interlaminated with micrite and occur as flocculated aggregates dispersed throughout laminated micrite (Fig. 6B). Silty carbonate (Fig. 6C) is identified in one sample of the Las Aguaditas Formation. Allochems in the Las Aguaditas Formation are restricted to trilobite fragments, except in rare beds that contain fragments of brachiopods, trilobites, bryozoans, and sponge spicules (Fig. 6D). Recrystallization of micrite to fine-grained microspar generally occurs along bedding planes and within rare packstone beds. Disseminated pyrite is identified in the Las Aguaditas Formation, and occurs predominantly along bedding planes.

4.1.1. Evidence for secondary components

At least three generations of calcite veins are distinguished by cross-cutting relationships in the strata of the upper San Juan, Las Chacritas, and Las Aguaditas formations within the field area, and are likely associated with Andean orogenesis that resulted in uplift and exposure of these successions (Astini et al., 1995; Allmendinger and Judge, 2014). A small network of thin (~50 μm) dark-colored (in hand sample) veins represent the first stage of vein formation. These veins are cut by thin (< 1 mm) white veins (cf. Fig. 6A), which are, in turn, cross-cut by a third generation of thick (1-7 mm) white veins. All vein stages have sharp contacts with surrounding rock. In thin section the first stage of veins is characterized by fine-grained equant calcite spar. The larger thin white veins and the final generation of veins are both characterized by coarse,

calcite spar exhibiting competitive growth into the center of the veins (i.e. syntaxial growth; (Scholle and Ulmer-Scholle, 2003).

4.1.2. Cathodoluminescence petrography

Cathodoluminescence (CL) analysis of carbonate lithologies from the upper San Juan, Las Chacritas, and Las Aguaditas formations show a variety of luminescence characteristics. Overall, CL analyses revealed dully luminescent, fine-grained limestone with variably luminescent, spar filled fractures and voids. The upper San Juan Formation is characterized by a dark orange dully luminescent matrix with brightly luminescent to moderately luminescent skeletal grains. Luminescence of later stage veins in the San Juan Formation is variable, from brightly luminescent to non-luminescent, and shows the sharp contrast between the host limestone and vein-filling cement. Large veins are generally compositionally zoned, with highly luminescent calcite spar evolving to dully luminescent calcite spar as the vein was filled.

In the Las Chacritas Formation, micrite and fine-grained microspar exhibit dark orange luminescence, with only small fossil fragments showing brighter luminescence (Fig. 5E). The heterogeneous, yet uniform, luminescence within matrix components is attributed to presence of disseminated siliciclastic and clay-rich grains, which are non-luminescent. Skeletal grains in the Las Chacritas Formation generally exhibit dull luminescence, similar to matrix components; however, spar-filled sponge spicule molds and rare echinoderm fragments are brightly luminescent (Fig. 5E). Later stage veins in the Las Chacritas Formation appear similar to those observed in the underlying San Juan Formation, with predominantly brightly luminescent calcite spar in large veins (Figs. 5E and 5F), although non-luminescent calcite spar is observed in small veins (< 0.5 mm) and in the center of some of the larger veins.

Limestone of the Las Aguaditas Formation exhibits a uniform dark to moderate orange luminescence. As with the Las Chacritas Formation, micritic and microsparitic matrix phases of the Las Aguaditas Formation are uniformly heterogeneous (Fig. 6E), although the luminescence is slightly darker, which may reflect an increase in the proportion of non-luminescent clay minerals. Skeletal grains in the Las Aguaditas Formation generally are less luminescent than the surrounding matrix, except for molds of sponge spicules, which are filled with brightly luminescent cement (Fig. 6F). Luminescence of later stage calcite veins in the Las Aguaditas Formation is variable with both brightly luminescent large veins (Fig. 6E) and dull to moderately luminescent smaller veins (Fig. 6F). Luminescence characteristics of veins are distinct from that of adjacent carbonate phases.

4.1.3. Interpretation

Limestone of the San Juan, Las Chacritas, and Las Aguaditas formations consist largely of micritic and microsparitic, carbonate mudstone and wackestone. Petrographic fabrics observed in these successions are consistent with deposition in subtidal marine environments. The poorly laminated micrite of the Las Chacritas Formation with intermittent clay drapes on bedding planes suggests deposition in relatively quiet water, below fair-weather wave base, with wackestone and packstone intervals likely representing reworking of shallower-water facies during storm events. Increased clay content and lamination within mudstone facies combined with a paucity of grain-rich intervals in the Las Aguaditas Formation suggests deposition predominantly below storm wave base.

The primary depositional phase of these limestones is micrite and finely crystalline microspar. The absence of more coarsely crystalline phases suggests that these phases have

undergone only minimal diagenetic recrystallization, because the process of dissolution and reprecipitation typically results in significant grain coarsening. Coarse grained calcite cements occur only within grain-rich lithologies, or as vein-filling components. Fossil components in both formations are well preserved; however, distinct differences in the abundance and diversity of fossils is observed between the units. Fauna in the lower Las Chacritas Formation is like that of the underlying San Juan Formation; however, fauna in the upper Las Chacritas Formation are restricted to trilobite fragments and recrystallized sponge spicules. In the Las Aguaditas Formation, only trilobite fragments and sponge spicules are observed. This restriction in faunal diversity is consistent with deposition of the Las Chacritas and Las Aguaditas formations along a deepening slope away from a remnant carbonate platform.

Dull orange luminescence observed for the matrix of both the Las Chacritas and Las Aguaditas formations is consistent with minimal recrystallization. Variation in the luminescence of matrix material appears to be largely restricted to discrete fossil grains and silty regions. Although the veins identified provide evidence for multiple later-diagenetic episodes of fluid flow, CL analysis shows no clear evidence that fluids participated in the alteration of matrix components. Furthermore, generally dull luminescence of micritic and microsparitic matrix suggests recrystallization occurred during early seafloor diagenesis. Early diagenetic recrystallization of the matrix material on the seafloor would have been buffered by interstitial fluids, with compositions near that of the original seawater. Previous studies have considered these fine-grained components to be most likely to record “near primary” seawater geochemical compositions (Kaufman et al., 1991; Kah et al., 1999; Bartley et al., 2007).

4.2. Geochemical characterization of carbonate phases

4.2.1. Carbon and oxygen isotopic compositions

Geochemical results from the Las Chacritas River and Las Aguaditas Creek sections are reported in Tables 1 and 2 and summarized in Table 3. Overall carbon isotope compositions, range from −2.25 to +1.41 ‰ (Tables 1-3; Figs. 7, 8A, and 9A). $\delta^{13}C$ values of petrographically well-preserved micritic and microsparitic phases in the Las Chacritas River section range from −1.48 to +1.41 ‰ (Table 1). Secondary carbonate phases, represented by spar within coarse-grained lithologies in the Las Chacritas Formation, have $\delta^{13}C$ values that range from −1.10 to +0.44 ‰. $\delta^{13}C$ compositions of vein-filling cements in the Las Chacritas formation range from −1.45 to +0.69 ‰. Similarly, $\delta^{13}C$ values for micritic phases in the Las Aguaditas Formation range from −2.25 to +0.56 ‰ (Table 2). Secondary carbonate in the Las Aguaditas Formation ranges from −0.58 to +1.0 ‰. Carbon isotope compositions of vein-filling cements in the Las Aguaditas Formation range from −1.37 to +0.52 ‰.

The O-isotopic compositions of micritic phases in the Las Chacritas Formation range from −7.23 to −3.14 ‰ (Table 1). $\delta^{18}O$ compositions for secondary carbonate (spar) range from −6.94 to −3.02 ‰. Vein-filling cements have $\delta^{18}O$ compositions ranging from −8.80 to −4.53 ‰. In the Las Aguaditas Formation, $\delta^{18}O$ compositions for micritic phases range from −5.81 to −4.06 ‰ (Table 2). Oxygen isotope compositions of sparry calcite in the Las Aguaditas Formation range from −5.44 to −3.22 ‰. Vein-filling cements in the Las Aguaditas Formation have oxygen isotope compositions ranging from −10.76 to −2.88 ‰.

4.2.2. Elemental signatures

Major- and trace-element chemistry of microdrilled carbonate phases were analyzed for Ca, Mg, Sr, Fe, and Mn concentrations (Tables 1 and 2, Figs. 8 and 9). All carbonate phases

from the Las Chacritas and Las Aguaditas formations have Mg/Ca ratios of less than 0.07, consistent with stoichiometric calcite. Strontium concentrations of matrix components in the Las Chacritas Formation range from 174 to 1330 ppm with an average concentration of 530 ± 252 ppm (n = 94; Table 1). Secondary carbonate spar has Sr concentrations from 190 to 585 ppm with an average of 363 ± 99 ppm (n = 20). Vein filling cements have Sr concentrations from 204 to 1383 ppm with an average concentration of 587 ± 278 ppm (n = 23). Manganese and iron concentrations in the Las Chacritas Formation range from 98 to 1553 ppm and 421 to 11,496 ppm with average values of 476 ± 196 and 2546 ± 1898 ppm (n = 94), respectively. Secondary calcite spar in the Las Chacritas Formation has concentrations ranging from 213 to 773 ppm and 492 to 3854 ppm with average values of 521 ± 156 and 1398 ± 772 ppm (n = 20) respectively for Mn and Fe.

Similarly, petrographically well-preserved micrite in the Las Aguaditas Formation has Sr concentrations ranging from 283 to 2166 ppm with an average of 788 ± 402 ppm (n = 80; Table 2). Strontium concentrations from secondary calcite phases, spar- and vein-filling cements, in the Las Aguaditas Formation range from 207 to 994 ppm and 278 to 1434 ppm with average concentrations of 467 ± 198 ppm (n = 28) and 781 ± 333 ppm (n = 23), respectively. Manganese and Fe concentrations of micritic carbonate in the Las Aguaditas Formation range from 163 to 3274 ppm and 525 to 6715 ppm with average concentrations of 642 ± 618 ppm and 6815 ± 2668 ppm (n = 80), respectively. Secondary carbonate (spar) from the Las Aguaditas Formation has Mn and Fe concentrations ranging from 206 to 2318 ppm and 278 to 6644 ppm with average concentrations of 549 ± 519 and 2264 ± 1688 ppm (n = 28), respectively. Later vein-filling cements in the Las Aguaditas Formation have Mn and Fe concentrations ranging from 156 to

1512 ppm and 278 to 6992 ppm with average concentrations of 561 ± 349 ppm and 3877 ± 1711 ppm (n = 23), respectively.

4.2.3. Interpretation

Carbonate minerals are chemically reactive and therefore susceptible to dissolution and recrystallization both syndepositionally, in the presence of seawater or modified pore fluids, and during later diagenesis in the presence of non-native fluids. Cross-plots of isotopic ($\delta^{13}C$ and $\delta^{18}O$) and elemental (Ca, Mg, Sr, Mn, and Fe) data provide a useful tool for assessing systematic variation associated with diagenetic alteration, because the degree of chemical alteration resulting from water-rock interaction has predictable behaviors (cf. Banner and Hanson, 1990). Potential end-member fluid compositions can further be inferred by comparing the geochemical composition of fine-grained depositional phases, such as micrite and microspar, and secondary carbonate phases, such as coarsely crystalline, vein-filling cement.

Carbon and oxygen compositions of depositional and diagenetic carbonate phases are shown in Figure 7. Carbon isotope compositions of depositional phases within both the Las Chacritas and Las Aguaditas formations fall broadly between −1.5 ‰ and +1.5 ‰, which is consistent with Darriwilian-aged carbonates worldwide (Ainsaar et al., 2004; Saltzman and Young, 2005; Kaljo et al., 2007; Schmitz et al., 2010; Zhang et al., 2010; Thompson et al., 2012; Albanesi et al., 2013; Edwards and Saltzman, 2016). Oxygen isotope compositions, similarly, fall largely between −4.5 ‰ and −6 ‰, which is consistent with well-preserved marine carbonate rocks of the lower Paleozoic (Carpenter and Lohmann, 1997; Veizer et al., 1999; Jaffrés et al., 2007). There are no discrete trends indicative of isotopic resetting resulting from interaction of carbonate minerals with meteoric waters, which are often characterized by

depletion in both ^{13}C and ^{18}O (Marshall, 1992). There is, however, a noted difference in composition between micrite-dominated matrix phases and more grain-rich matrix phases, which contain a greater amount of intergranular sparry cement. Micrite-dominated phases in both the Las Chacritas and Las Aguaditas formations have lower carbon and oxygen isotope compositions, by ~ 1 ‰ and 0.5 ‰ respectively. Although this difference in isotopic composition is small, its correspondence to lithologies that are inferred to represent shallower (grain-rich) and deeper (micrite-dominated) depositional environments suggest different diagenetic pathways. Possibilities include: (1) the presence of primary differences in the composition of shallower and deeper water bodies, (2) differences in primary porosity leading to early diagenetic stabilization by isotopically different fluids (i.e., seawater for grain-rich phases, and modified substrate pore fluids for micritic phases; cf. Schrag et al., 2013), or (3) preferential alteration of specific phases in the presence of late diagenetic fluids.

Examination of the Las Chacritas and Las Aguaditas formations separately (Figs. 8A and 9A) reveals that there is no consistent pattern between the composition of primary phases and that of secondary calcite phases, which is consistent with only minimal isotope exchange between carbonate minerals and later diagenetic fluids. This observation is consistent with an interpretation in which the isotopic variation between micrite and grain-rich lithologies reflects a primary difference in the composition of early diagenetic fluids.

Trace elements incorporated into carbonate phases can provide additional insight into the depositional and diagenetic history of these samples. Strontium concentrations of carbonate rocks, in particular, are easily altered during diagenetic recrystallization (Brand and Veizer, 1980; Banner and Hanson, 1990). In both the Las Chacritas and Las Aguaditas formations (Figs. 8B and 9B), there is no clear relationship between the Sr concentration of depositional phases

and that of vein mineralization, which supports an interpretation of only minimal isotopic exchange during late-stage diagenesis. Strontium concentrations in both formations are consistently lower in grain-rich lithologies, suggesting potential for a greater degree of early diagenetic recrystallization. In both formations, however, grain-rich lithologies average 313 ± 60 ppm Sr, which is similar to that expected from calcite precipitated from open marine waters (Veizer, 1983). More elevated Sr concentrations (> 1000 ppm) within micritic lithologies, along with $\delta^{18}O$ compositions typical of well-preserved marine carbonate, suggests minimal recrystallization of primary carbonate phases. Secondary carbonate phases with Sr concentrations similar to those of primary phases further suggest the limestone of the Las Chacritas and Las Aguaditas formations have not undergone significant diagenetic recrystallization, because Sr is commonly excluded from the crystal lattice with recrystallization, even at low water-rock ratios. Combined, the fabric retentive nature of carbonate phases in the Las Chacritas and Las Aguaditas formations, combined with these observations suggest that recrystallization of matrix phases likely occurred in penecontemporaneous marine or modified marine fluids.

Elevated concentrations of redox-sensitive trace elements, such as Mn and Fe, can be used as evidence for recrystallization of carbonate phases in reducing fluids associated with deep-burial (Veizer, 1983). Low concentrations of Mn and Fe, however, are expected for carbonate phases derived from oxygenated marine waters, and higher concentrations may reflect deposition or early diagenetic stabilization in sub-oxic to anoxic fluids. Manganese concentrations of depositional carbonate phases in the Las Chacritas and Las Aguaditas formations are typically < 500 ppm, although concentrations reach as high as 1553 ppm in the Las Chacritas Formation and 3274 ppm in the Las Aguaditas Formation. Iron concentrations are

even more variable (Figs. 8C and 9C). Elevated Mn and Fe concentrations co-occur with Sr concentrations that indicate limited alteration of marine carbonate phases. Combined with interpretations of deposition during flooding of the San Juan platform, suggesting that elevated Mn and Fe concentrations may record incorporation of these elements during precipitation of early diagenetic stabilization of carbonate in anoxic marine fluids or pore waters (cf. Thompson and Kah, 2012; Gilleaudeau and Kah, 2013).

Combined, these observations suggest deposition and early diagenetic stabilization of carbonate lithologies of the Las Chacritas and Las Aguaditas formations in sub-oxic to anoxic marine fluids or marine pore waters. These samples likely preserve carbon isotope values that reflect their environments of deposition and early diagenetic stabilization; resetting of carbon isotope values typically requires extensive water-rock interaction not supported by the preserved isotopic and elemental compositions (Banner and Hanson, 1990). Even under the assumption that elevated Mn concentrations reflect recrystallization during later diagenesis, Mn/Sr ratios as high as 10 have been shown to retain near primary marine carbon isotope compositions (Kaufman and Knoll, 1995). Depositional carbonate phases in the Las Chacritas and Las Aguaditas formations (Figs. 8D and 9D) generally have Mn/Sr < 1. Samples with Mn/Sr > 1 occur in the uppermost strata of the San Juan Formation in both sections, suggesting a possible stratigraphic control on Sr and Mn concentrations. There is no petrographic evidence of differential diagenesis in these samples; however, these carbonates were deposited during marine transgression, which is consistent with elevated Mn concentrations potentially associated with transgression of deeper, anoxic marine fluids across the shelf.

4.3. Carbon isotope compositions of organic matter

Sedimentary organic matter ranges from 0.04 to 0.53 wt. % in the Las Chacritas Formation and from 0.03 to 0.36 wt. % in the Las Aguaditas Formation. The carbon isotope composition of organic matter is similar in both units, ranging between −30.45 to −24.16 ‰ in the Las Chacritas Formation and −30.84 to −22.76 ‰ in the Las Aguaditas Formation.

4.3.1. Interpretation

Photosynthetic production of organic matter from the marine DIC pool results in organic matter depleted in ^{13}C by approximately 22–30 ‰ (Hayes et al., 1999), which is consistent with isotopic compositions observed within the Las Chacritas and Las Aguaditas formations. Carbon isotope compositions of marine organic matter, however, can also be affected by diagenetic alteration, terrestrial organic input, and heterotrophic reworking within the depositional environment. For example, the isotopic composition of sedimentary organic carbon may be affected by thermal maturation and post-depositional fluid flow that results in isotopically heavier $\delta^{13}C_{org}$ compositions (Hayes et al., 1999; Derry, 2010). Approximate burial temperatures for the Las Chacritas and Las Aguaditas formations are provided by conodont elements, which have conodont alteration indices of 2.5–3 (Serra et al., 2015; Feltes et al., 2016), corresponding to burial temperatures between 90–190˚C (Epstein et al., 1977). Differences in thermal histories for the Las Chacritas and Las Aguaditas formations may explain some of the $\delta^{13}C_{org}$ variation between these formations; however, it does not explain stratigraphic changes in $\delta^{13}C_{org}$ in a single outcrop where a uniform thermal history is expected.

Although purported terrestrially derived organic carbon has been identified in Darriwilian strata (cf. Strother et al., 1996), such material is rare and the isotopic composition of this organic carbon (~ −29 ‰; Jahren et al., 2003) is unlikely to be easily differentiated from marine organic

carbon, and is, therefore, not further considered. Finally, remineralization of organic carbon by heterotrophic metabolic activities in the substrate can result in either isotopic enrichment, through aerobic oxidation of organic matter under well-mixed and oxygenated conditions, or isotopic depletion, via secondary input of isotopically light organic carbon via chemoautotrophic microbial metabolisms (cf. Hayes et al. 1999; further discussed in Section 5).

4.4. Chemostratigraphic profiles

Petrographic, isotopic, and elemental data suggest that the Las Chacritas and Las Aguaditas formations likely retain near-primary marine geochemical signatures, associated with deposition and early diagenetic stabilization at or near the sediment-water interface. Chemostratigraphic profiles for the Las Chacritas and Las Aguaditas formations are shown in Figure 10. In the Las Chacritas section, $\delta^{13}C_{carb}$ increases from around −1 ‰ to around 0 ‰ at the top of the *L. variabilis* Zone within the San Juan Formation. In the *Y. crassus* Zone, $\delta^{13}C_{carb}$ is relatively stable around −1 ‰, with values of −0.73 ± 0.26 ‰ in the lower *Y. crassus* Zone, and −0.90 ± 0.29 ‰ in the upper *Y. crassus* zone (Fig. 10). $\delta^{13}C_{carb}$ compositions then steadily increase from around −1 ‰ to +0.5 ‰ through the *E. pseudoplanus* Zone before reaching a high of +1.4 ‰ in the basal *E. suecicus* Zone. $\delta^{13}C_{carb}$ values return to near 0 ‰ in the *P. anserinus* Zone.

At the Las Aguaditas Creek section, $\delta^{13}C_{carb}$ values in the *Y. crassus* Zone (here representing the uppermost San Juan Formation and lowermost Las Aguaditas Formation) are similar to values recorded in the Las Chacritas creek section, with values of −0.31 ± 0.20 ‰ in the lower *Y. crassus* Zone, and −0.61 ± 0.25 ‰ in the upper *Y. crassus* Zone. By contrast, $\delta^{13}C_{carb}$ compositions in the *E. pseudoplanus/D. tablepointensis* Zone of the Las Aguaditas

Formation, rather than rising to positive values, abruptly fall to values of −1.15 ± 0.52 ‰. An abrupt transition to $\delta^{13}C_{carb}$ values near 0.25 ‰ marks the *P. anserinus* Zone.

The $\delta^{13}C_{org}$ record is more variable. In the uppermost strata of the San Juan Formation, $\delta^{13}C_{org}$ values are relatively stable ~ −29 ‰ and increase in the Las Chacritas Formation to values near −28 ‰ through the *Y. crassus* Zone and the lower *E. pseudoplanus* Zone (Fig. 11). Variability in $\delta^{13}C_{org}$ increases in the transition from the *Y. crassus* to the *E. pseudoplanus* zones, with values ranging between −24.16 and −29.79 ‰. $\delta^{13}C_{org}$ then records an abrupt decrease to values near −30 ‰ through remainder of the *E. pseudoplanus* Zone and within the *E. suecicus* Zone. Values remain near −30 ‰ in the *P. anserinus* Zone.

The $\delta^{13}C_{org}$ record of the Las Aguaditas Formation is more variable than the shallower water Las Chacritas Formation. At the Las Aguaditas Creek Section, $\delta^{13}C_{org}$ values from the lower *Y. crassus* Zone in the San Juan Formation are variable around −26 ‰, before abruptly falling to values that remain near −30 ‰ in the upper *Y. crassus* Zone. $\delta^{13}C_{org}$ values, although more variable, remain near −30 ‰ in the *E. pseudoplanus/D. tablepointensis* Zone. Above the unconformity at the top of the lower member of the Las Aguaditas Formation values increase to around −26 ‰ before falling to around −31 ‰.

5. Discussion

5.1. Summary of observations

The Las Chacritas and Las Aguaditas formations reflect deposition during the *Y. crassus* and *E. pseudoplanus* conodont biozones (Darriwilian, Dw2) and the lowermost *E. suecicus* Zone (Darriwilian, Dw3), which include the timeframe of the globally recognized MDICE (Meidla et al., 2004; Ainsaar et al., 2007; Schmitz et al., 2010; Zhang et al., 2010; Thompson et al., 2012;

Albanesi et al., 2013; Edwards and Saltzman, 2014; Kah et al., 2016; Young et al., 2016). Combined petrographic and geochemical data from the Las Chacritas and Las Aguaditas formations suggest early diagenetic stabilization of micritic carbonate phases at or near the seafloor in the presence of marine, or potentially modified marine, porewaters with little evidence for alteration of chemical compositions by late diagenetic fluids. Within this framework, we explore the origin of distinct isotopic patterns between coeval shallower-water facies of the Las Chacritas Formation and deeper-water facies of the Las Aguaditas Formation through the MDICE interval.

The isotopic composition of marine carbonate recorded in the Las Chacritas and Las Aguaditas formations show a similar stable trend through the *Y. crassus* Zone, although $\delta^{13}C_{carb}$ values are heavier in the Las Aguaditas Formation by approximately 0.4 ‰ (Fig. 10). During the MDICE interval, which occurs within the *E. pseudoplanus* and *E. suecicus* Zones, the Las Chacritas Formation records $\delta^{13}C_{carb}$ values increasing from around −1.0 ‰ to around +1.0 ‰. Whereas Albanesi et al. (2013) measured bulk $\delta^{13}C_{carb}$ values of marine carbonate, which can result in the mixing of early and late diagenetic phases, our microsampling of discrete carbonate phases yields data suggesting the expression of the MDICE is stronger in the Precordillera than previously recognized. The ~ 2.0 ‰ positive shift in $\delta^{13}C_{carb}$ values recorded in the Las Chacritas Formation is comparable to the global expression of the MDICE, which ranges from ~ 1 ‰ in China (Schmitz et al., 2010; Kah et al., 2016), to ~ 1.5 ‰ in Estonia (Meidla et al., 2004; Ainsaar et al., 2007; Kaljo et al., 2007) and Newfoundland (Thompson and Kah, 2012), to ~ 2.5 ‰ in Nevada, USA (Young et al., 2016) and Sweden (Calner et al., 2014), and to up to ~ 4 ‰ in Maryland, USA (Leslie et al., 2011), despite the erosional removal of the upper *E. suecicus* Zone.

By contrast, the MDICE interval in time equivalent strata of the Las Aguaditas Formation is characterized by an abrupt shift to values near −1.5 ‰. To our knowledge the Las Aguaditas Formation provides the first clear divergence from the globally observed positive isotopic shift. Previous work in the Las Aguaditas Formation recognized carbon isotope composition near −1 ‰ through the MDICE interval (Albanesi et al., 2013), but attributed the lack of a clear MDICE signal to removal of strata associated with the top of the *E. pseudoplanus* and *E. suecicus* conodont zones. However, recent biostratigraphic analysis identified the *Histiodella kristinae* Subzone in the uppermost strata of the Lower Member of the Las Aguaditas Formation, which is commonly associated with the *E. suecicus* zone, although the *E. suecicus* Zone is not formally recognized in the Las Aguaditas Formation (Serra et al., 2015; Feltes et al., 2016). Therefore, the MDICE, or at least the initiation of the MDICE interval, should be present in both formations.

The presence of stratigraphically younger conodonts in the *E. suecicus* Zone in the Las Chacritas Formation (*Histiodella bellburnensis*; Serra et al., 2015) and the lack of this zone in the Las Aguaditas Formation suggests that the regional disconformity identified at the top of each section represents less time in shallower-water depositional environments. This is consistent with oblique convergence of the Precordillera terrane and associated uplift and erosion of strata associated with migration of the peripheral bulge (cf. Astini et al., 1995).

5.2. Potential for geochemical alteration

The presence of a regional disconformity suggests the possibility that geochemical signatures preserved in the Las Chacritas and Las Aguaditas formations may be affected by diagenetic overprinting from isotopically depleted waters during subaerial exposure. C-isotope compositions that are depleted in ^{13}C have been identified beneath subaerial exposure surfaces

identified in Neoproterozoic to Cenozoic carbonate successions (Beeunas and Knauth, 1985; Andrews, 1991; Sarkar et al., 1998; Railsback et al., 2003; Banerjee et al., 2006). Such isotopic depletions can be as large as 4-6 ‰ at the exposure surface and become smaller at depth (Allan and Matthews, 1982). Subaerial exposure also commonly leads to covariant trends in $\delta^{13}C_{carb}$ and $\delta^{18}O$ (Knauth and Kennedy, 2009), because meteoric fluids are commonly depleted in both ^{13}C (Derry, 2010) and ^{18}O (Bowen and Wilkinson, 2002). Interaction of carbonate minerals with meteoric fluids during subaerial exposure also typically yield a decrease in Sr concentrations, reflecting both the propensity for Sr to be rejected from the carbonate lattice during recrystallization (Brand and Veizer, 1980) and the relatively low Sr concentration of terrestrial fluids (Banner, 1995).

In the Las Aguaditas Formation, petrographic and geochemical data suggest little interaction with late diagenetic fluids. Carbonate mudstone and wackestone within this interval is petrographically well preserved and lacks both petrographic or cathodoluminescent evidence of grain coarsening associated with dissolution and reprecipitation reactions. Strontium concentrations in this interval are some of the highest in the formation (averaging 1175 ± 400 ppm, n = 20), which is inconsistent with extensive diagenetic alteration by meteoric or other post-depositional fluids (Fig. 9B; Table 2). Furthermore, the strata beneath the unconformity contain elevated concentrations of both Mn (378 ± 90 ppm; n = 12; Fig. 9C) and Fe (378 ± 90 ppm and 2373 ± 1459 ppm; n = 12), which is inconsistent with alteration by well oxygenated surface fluids (Lohmann, 1988).

5.3. Potential for recovery of gradients in ocean chemistry

A number of high-resolution geochemical studies have explored the potential for spatial heterogeneity of the marine carbon isotope record (Gilleaudeau and Kah, 2013; Edwards and Saltzman, 2016; Saltzman and Edwards, 2017), especially within epicratonic seas, where carbonate rocks have been shown to exhibit a systematic reduction in $\delta^{13}C_{carb}$ compositions, when compared to coeval pericratonic and offshore marine environments (Holmden et al., 1998; Panchuk et al., 2006). Aerobic activity in surface waters would lead to enhanced organic matter oxidation by heterotrophic microorganisms and increased redox stratification of the water column in the Early-Middle Ordovician (cf. Kah et al., 2016). Under low oxygen conditions, Mn and Fe are readily reduced through microbial processes either within the water column or within substrate pore fluids (Thamdrup et al., 2000), where they can then be incorporated into carbonate minerals. Carbonate minerals with elevated Mn and Fe concentrations and little petrographic evidence of post-depositional recrystallization have been used to argue for deposition under low oxygen conditions (Kah et al., 2012; Thompson and Kah, 2012; Gilleaudeau and Kah, 2013; Guo et al., 2013). Such a scenario is consistent with elevated concentrations of Mn and Fe, combined with elevated Sr and an absence of petrographic evidence for substantial post-depositional recrystallization, in the Las Chacritas and Las Aguaditas formations suggesting deposition of both of these units near a marine chemocline.

Combined, petrographic and geochemical data suggest little post-depositional alteration of micritic carbonate phases from the Las Chacritas and Las Aguaditas formations and thus, are likely reflect early diagenetic stabilization in seawater or seawater modified by microbial activity within the shallow substrate. In this case, an abrupt divergence in $\delta^{13}C_{carb}$ compositions between the Las Chacritas and Las Aguaditas formations suggest that facies may be sampling geochemically distinct parts of the marine water column through the MDICE interval. Here we

suggest that an abrupt shift in the carbon isotopic composition of the Las Aguaditas at the initiation of the MDICE may reflect variation in the composition of marine DIC in carbonate deposited at or near a marine chemocline.

Relative isotopic stasis in the $\delta^{13}C_{carb}$ record of both the Las Chacritas and Las Aguaditas formations prior to the MDICE interval (Fig. 10) is consistent with deposition in a well-mixed water column (cf. Fig. 12). In a well-mixed oxygenated water column, isotopically depleted photosynthetic organic matter produced in surface waters ($\delta^{13}C_{org}$ ~ −25 to −30 ‰; Freeman et al., 2001) and removed as sedimentary organic carbon. Organic carbon burial results in ^{13}C enrichment of DIC, which is incorporated into marine carbonate minerals with minimal isotopic fractionation (Spero et al., 1997), driving the positive excursion in $\delta^{13}C_{carb}$ compositions of the Las Chacritas Formation. Remineralization of organic carbon in well-oxygenated waters and within the shallow substrate by aerobic marine heterotrophs, typically results in a small positive shift (~ 1.5 ‰; Hayes et al., 1989) in $\delta^{13}C_{org}$ compositions and the formation of isotopically light CO_2 (Hayes et al., 1989). More extensive remineralization of sedimentary organic carbon in substrate underlying oxygenated waters can result in both a shift toward isotopically light organic carbon (up to several ‰; cf. Guo et al., 2013) and incorporation of isotopically light CO_2 into carbonate minerals (cf. Schrag et al., 2013). This may explain the observed ~ 0.5 ‰ offset in $\delta^{13}C_{carb}$ compositions between the Las Chacritas and the Las Aguaditas formations prior to the MDICE. The Las Chacritas Formation does not record evidence for either substantial microbial remineralization (Fig. 11) or incorporation of isotopically light DIC (Fig. 10) through either the *Y. crassus* or *E. pseudoplanus* zones which is consistent with deposition and early diagenetic stabilization of micrite above the oxycline.

By contrast, the Las Aguaditas Formation records an abrupt shift in $\delta^{13}C_{org}$ compositions to more negative values prior to the onset of the MDICE (Fig. 11). The shift to isotopically light $\delta^{13}C_{org}$ compositions in the Las Aguaditas Formation is also associated with greater volatility in $\delta^{13}C_{carb}$ values in the uppermost *Y. crassus* Zone, and with an abrupt shift in $\delta^{13}C_{carb}$ compositions in the *E. pseudoplanus* Zone at the start of the MDICE (Fig. 10). This shift is associated with an increase in deeper-water facies and suggests the presence of active microbial remineralization of organic matter either within the water column, or within the shallow substrate and is interpreted to reflect strengthening of the oxycline and deposition of the Las Aguaditas Formation below the oxycline. Minimal grain coarsening within micrite and enrichment of Mn and Fe from anoxic marine fluids is consistent with early diagenetic stabilization of carbonate below the oxycline. When the Las Aguaditas Formation falls below the oxycline, $\delta^{13}C_{carb}$ is offset by ~2 ‰ from coeval shallow water carbonate record of the Las Chacritas Formation, reflecting the input of isotopically depleted DIC resulting from microbial metabolisms in anoxic water. A similar shift is observed in the Las Chacritas section in the *E. suecicus* Zone and the *P. anserinus* Zone, which records deposition of deeper-water facies of the Las Chacritas and Las Aguaditas formations (Figs. 10 and 11). Correspondence between isotopic shifts in both organic carbon and marine carbonate in the Las Aguaditas Formation support an interpretation that isotopic differences between the Las Chacritas and Las Aguaditas sections reflect the presence of an oxycline and the local production of isotopically light DIC pool.

5.4. Implications for the redox structure of Middle Ordovician oceans

A scenario of deposition at or near a marine chemocline is consistent with growing model for the behavior of the Ordovician ocean. In this model persistent greenhouse conditions from

the Cambrian through the Middle Ordovician (Saltzman, 2005), combined with low-latitude continental positions (Cocks and Torsvik, 2002), and high global sea level (Haq and Schutter, 2008) would have shifted the location of bottom water formation to low-latitude epeiric seas resulting in the formation of warm-saline deep water (Railsback et al., 1990). Formation of saline deep-water in low- to mid-latitude evaporative seas, rather than in polar regions as in the modern ocean (Foster and Carmack, 1976; England, 1992), would result in a reduction in both thermal and density gradients of the ocean, effectively reducing the rate of ocean mixing between well-mixed surface and deep-water bodies (Railsback et al., 1990). Because the isotopic composition of marine DIC reflects a balance of continental runoff, surface gas exchange with the atmosphere, and remineralization of organic carbon the water column and sediment pore fluids (Zhang et al., 1995), differences in the C-isotope composition of DIC between surface waters and deeper water in the ocean are dependent on the degree and rate of mixing between deeper water and well-mixed surface water (Patterson and Walter, 1994). Under conditions marked by reduced mixing, biogeochemical cycling would then result in pronounced geochemical gradients. Additionally, reduction of oxygen solubility during greenhouse periods would have further reduced oxygen concentrations at depth, potentially leading to redox stratification of the water column (Küspert, 1982; Railsback et al., 1990).

Development of a marine chemocline, with well-mixed oxygenated surface waters and oxygen depleted to anoxic deep waters, has been previously linked to excursions in the isotopic compositions of marine carbon in the Paleozoic (Knoll et al., 1996; Saltzman, 2005; Thompson and Kah, 2012; Marenco et al., 2013; Kah et al., 2016). Specifically, stasis in $\delta^{13}C$ compositions during the early Paleozoic greenhouse has been attributed to nitrogen limitation, which promotes denitrification and subsequent development of anoxic conditions in the water column (Saltzman,

2005). Under anoxic conditions, phosphorus is more easily remobilized from sediments to the water column leading to increased productivity, burial of organic carbon, and subsequent positive $\delta^{13}C$ excursions (Saltzman, 2005). Positive $\delta^{13}C$ excursions (e.g., SPICE, MDICE, and HICE) are then associated with upwelling of nutrient-rich deep waters into shallow water environments (Van Cappellen and Ingall, 1994; Pope and Steffen, 2003; Servais et al., 2014), resulting in enhanced organic productivity of surface waters.

5.5. Depositional scenarios

The carbon isotope record of carbonate and organic matter from the Las Chacritas and Las Aguaditas formations suggest deposition near the oxycline. Relatively stable $\delta^{13}C_{carb}$ values and $\delta^{13}C_{org}$ values of −26 to −28 ‰ in the lower *Y. crassus* Zone of both sections suggests deposition of strata above the oxycline (Fig. 12). An abrupt shift to lower $\delta^{13}C_{org}$ values (near −30 ‰) at the onset of the Las Aguaditas Formation suggests a shift to deposition at or below the oxycline. Continuation of distinctly lower $\delta^{13}C_{org}$ values in the Las Aguaditas Formation, and increased volatility of $\delta^{13}C_{org}$ values in the Las Chacritas Formation in the *E. pseudoplanus* Zone suggests that the marine chemocline may, during this time, be affecting both sections, although preservation of the MDICE suggests that the Las Chacritas River section remained above the oxycline. Finally, an abrupt shift to lower $\delta^{13}C_{org}$ values (near −30 ‰) in the *E. suecicus* Zone of the Las Chacritas River section suggests that by the late Darriwilian, deposition in both the Las Chacritas River and Las Aguaditas Creek sections occurred beneath the marine chemocline as carbonate production was unable to keep up with sea level rise (Fig. 12).

Through each of these transitions a change in the relative position of the oxycline is required to drive the observed isotopic change. Three such mechanisms are possible. In the first

scenario, enhanced nutrient delivery resulting from continental weathering may have increased productivity in surface waters, resulting in expansion of marine anoxia and shoaling of the oxycline at the onset of deposition of the Las Aguaditas Formation. Although this model is consistent with the observed $\delta^{13}C_{carb}$ and $\delta^{13}C_{org}$ compositions for the Las Chacritas and Las Aguaditas formations, it is inconsistent with sedimentological evidence for abrupt deepening at the onset of Las Aguaditas deposition. It is also unlikely that marine anoxia would be able to persist in environments that contain evidence for storm mixing, such as those inferred for the uppermost San Juan Formation and Las Chacritas Formation. Furthermore, this scenario is inconsistent with sulfur isotope evidence from the middle Darriwilian (Kah et al., 2016). Rapid fluctuations in the $\delta^{34}S$ composition of marine sulfate, differential rates of change in the isotopic composition of marine sulfate and sulfide, and the occurrence of "superheavy" pyrite have been used to argue for increased ventilation of a persistent anoxic water body in the middle Darriwilian (Thompson and Kah, 2012; Marenco et al., 2013; Kah et al., 2016).

In a second scenario, relative sea level rise through the middle Darriwilian results in a shift in the position of the Las Aguaditas Formation to below the marine chemocline (Fig. 12). This scenario is consistent with sedimentological evidence from the Las Chacritas River and Las Aguaditas Creek sections, and may be explained either by an inferred global sea level rise in the middle Darriwilian (~ 464 Ma, Haq et al., 2008), or preferential subsidence of the Precordilleran margin associated with the initial docking of the Precordilleran terrane to Gondwana (Astini et al., 1995; Astini and Thomas, 1999; Thomas et al., 2002).

In a final scenario, in addition to a relative change in sea level, global cooling through the Early to Middle Ordovician (Trotter et al., 2008) could have invigorated thermohaline circulation, potentially leading to ventilation of anoxic deep-water. Prior to this hypothesized

ventilation event, ocean stratification would result in the formation of isotopically light DIC in deep water. Subsequent intrusion of deeper water into shallow water environments in the middle Ordovician, via upwelling or ventilation, would reintroduce this isotopically light carbon into the shallow-water DIC pool along with bio-essential nutrients. Increased productivity in surface waters would then trigger increased productivity and organic carbon burial, ultimately resulting in the MDICE. Upwelling of ^{13}C depleted DIC from deep water may impart a localized signal on the isotopic compositions closest to the zone of upwelling (Patterson and Walter, 1994). Isotopic depletion during upwelling is expected to be greatest along the upwelling front, where upwelling water first comes into contact with surface water (Panchuk et al., 2006), resulting in isotopic depletion in the area closest to the chemocline (Kolata et al., 2001), which may be reflected in the increased isotopic volatility in the MDICE interval seen here.

6. Conclusions

Recent revisions to the biostratigraphy of the Middle Darriwilian Las Chacritas and Las Aguaditas formations in the Argentine Precordillera indicate that both formations should record the presence of the MDICE interval, or at least its initiation. We investigated the expression of the MDICE across depositional environments within a single basin. We identify the MDICE as a positive 2 ‰ shift in carbonate in the *E. pseudoplanus* and *E. suecicus* zones in the Las Chacritas Formation, while equivalent strata in the deeper water Las Aguaditas Formation record an abrupt decrease in the isotopic composition of marine carbonate. To our knowledge, this is the first recording of isotopic compositions during the MDICE interval that diverge from the global positive isotopic excursion. Paired carbon isotope from marine carbonate and organic carbon suggest that divergent behavior of the MDICE interval results from deposition above and below

a marine chemocline. Sedimentological differences between the Las Chacritas and Las Aguaditas formations suggest the presence of a persistent oxycline just below storm wave base, with differences in the isotopic behavior of the two sections related to their position relative to this marine chemocline.

Acknowledgments

We thank Thomas Algeo, Cole Edwards, and an anonymous reviewer for their thoughtful improvements to this manuscript. Funding for this projected was provided by the New Directions grant from the American Chemical Society Petroleum Research Fund (to Kah), along with student grants from Sigma Xi, the Geological Society of America, and SEPM (to Henderson). We thank R. Bales (University of Tennessee), and M. Mango (University of Cordoba) for assistance with fieldwork; A. Faiia and A. Szynkiewicz (University of Tennessee) for help with isotopic analyses; and the University of Tennessee Department of Chemistry for access to the ICP-OES.

References:

Ainsaar, L., Meidla, T., Tinn, O., 2004. Middle and Upper Ordovician stable isotope stratigraphy across the facies belts in the East Baltic, in: Hints, O., Ainsaar, L. (Eds.), 8th Meeting on the Working Group on the Ordovician Geology of Baltoscandia. Tartu University Press, Tallinn and Tartu, Estonia, pp. 11-12.

Ainsaar, L., Meidla, T., Tinn, O., Martma, T., Dronov, A., 2007. Darriwilian (Middle Ordovician) carbon isotope stratigraphy in Baltoscandia. Acta Paleontologica Sinica 46, 1-8.

Albanesi, G.L., Barnes, C.R., 2000. Subspeciation within a Punctuated Equilibrium Evolutionary Event: Phylogenetic History of the Lower-Middle Ordovician *Paroistodus originalis-P. horridus* Complex (Conodonta). Journal of Paleontology 74, 492-502. https://doi.org/10.1666/0022-3360(2000)074%3C0492:SWAPEE%3E2.0.CO;2

Albanesi, G.L., Bergström, S.M., Schmitz, B., Serra, F., Feltes, N.A., Voldman, G.G., Ortega, G., 2013. Darriwilian (Middle Ordovician) $\delta^{13}C_{carb}$ chemostratigraphy in the Precordillera of Argentina: Documentation of the middle Darriwilian Isotope Carbon Excursion (MDICE) and its use for intercontinental correlation. Palaeogeography, Palaeoclimatology, Palaeoecology 389, 48-63. http://dx.doi.org/10.1016/j.palaeo.2013.02.028

Albanesi, G.L., Ortega, G., 2016. Conodont and Graptolite Biostratigraphy of the Ordovician System of Argentina, in: Michael, M. (Ed.), Stratigraphy & Timescales. Academic Press, pp. 61-121. http://dx.doi.org/10.1016/bs.sats.2016.10.002

Allan, J.R., Matthews, R.K., 1982. Isotope signatures associated with early meteoric diagenesis. Sedimentology 29, 797-817. http://dx.doi.org/10.1111/j.1365-3091.1982.tb00085.x

Allmendinger, R.W., Figueroa, D., Snyder, D., Beer, J., Mpodozis, C., Isacks, B.L., 1990. Foreland shortening and crustal balancing in the Andes at 30˚- S latitude. Tectonics 9, 789-809. http://dx.doi.org/10.1029/TC009i004p00789

Allmendinger, R.W., Judge, P.A., 2014. The Argentine Precordillera: A foreland thrust belt proximal to the subducted plate. Geosphere 10, 1203-1218. http://dx.doi.org/10.1130/ges01062.1

Alvarez-Marron, J., Rodriguez-Fernandez, R., Heredia, N., Busquets, P., Colombo, F., Brown, D., 2006. Neogene structures overprinting Palaeozoic thrust systems in the Andean Precordillera at 30°S latitude. Journal of the Geological Society 163, 949-964. http://dx.doi.org/10.1144/0016-76492005-142

Andrews, J.E., 1991. Geochemical indicators of depositional and early diagenetic facies in Holocene carbonate muds, and their preservation potential during stabilisation. Chemical Geology 93, 267-289. http://dx.doi.org/10.1016/0009-2541(91)90118-B

Astini, R.A., 1995a. Geologic meaning of Arenig-Llanvirn diachronous black shales (Gualcamayo Alloformation) in the Argentine Precordillera, tectonic or eustatic? SEPM Fieldtrip Guidebook 77, 217-220.

Astini, R.A., 1995b. Sedimentología de la Formación Las Aguaditas (talud carbonático) y evolución de la cuenca precordillera durante el Ordovícico medio. Revista de la Asociación Geológica Argentina 50, 143-164.

Astini, R.A., Benedetto, J.L., Vaccari, N.E., 1995. The early Paleozoic evolution of the Argentine Precordillera as a Laurentian rifted, drifted, and collided terrane: A geodynamic model. Geological Society of America Bulletin 107, 253-273. https://doi.org/10.1130/0016-7606(1995)107%3C0253:TEPEOT%3E2.3.CO;2

Astini, R.A., Thomas, W.A., 1999. Origin and evolution of the Precordillera terrane of western Argentina; a drifted Laurentian orphan. Special Paper - Geological Society of America 336, 1-20. https://dx.doi.org/10.1130/0-8137-2336-1.1

Azmy, K., Stouge, S., Brand, U., Bagnoli, G., Ripperdan, R., 2014. High-resolution chemostratigraphy of the Cambrian–Ordovician GSSP: Enhanced global correlation tool. Palaeogeography, Palaeoclimatology, Palaeoecology 409, 135-144. http://dx.doi.org/10.1016/j.palaeo.2014.05.010

Banerjee, S., Bhattacharya, S.K., Sarkar, S., 2006. Carbon and oxygen isotope compositions of the carbonate facies in the Vindhyan Supergroup, central India. Journal of Earth System Science 115, 113-134. http://dx.doi.org/10.1007/bf02703029

Banner, J.L., 1995. Application of the trace element and isotope geochemistry of strontium to studies of carbonate diagenesis. Sedimentology 42, 805-824. http://dx.doi.org/10.1111/j.1365-3091.1995.tb00410.x

Banner, J.L., Hanson, G.N., 1990. Calculation of simultaneous isotopic and trace-element variations during water-rock interaction with applications to carbonate diagenesis. Geochimica et Cosmochimica Acta 54, 3123-3137. http://dx.doi.org/10.1016/0016-7037(90)90128-8

Bartley, J.K., Kah, L.C., McWilliams, J.L., Stagner, A.F., 2007. Carbon isotope chemostratigraphy of the Middle Riphean type section (Avzyan Formation, Southern Urals, Russia): Signal recovery in a fold-and-thrust belt. Chemical Geology 237, 211-232. http://dx.doi.org/10.1016/j.chemgeo.2006.06.018

Beaumont, C., 1981. Foreland basins. Geophysical Journal of the Royal Astronomical Society 65, 291-329. http://dx.doi.org/10.1111/j.1365-246X.1981.tb02715.x

Beeunas, M.A., Knauth, L.P., 1985. Preserved stable isotopic signature of subaerial diagenesis in the 1.2-b.y. Mescal Limestone, central Arizona: Implications for the timing and development of a terrestrial plant cover. Geological Society of America Bulletin 96, 737-745. http://dx.doi.org/10.1130/0016-7606(1985)96<737:psisos>2.0.co;2

Benedetto, J.L., 2004. The allochthony of the Argentine Precordillera ten years later (1993-2003): A new paleobiogeographic test of the microcontinental model. Gondwana Research 7, 1027-1039. http://dx.doi.org/10.1016/s1342-937x(05)71082-0

Benedetto, J.L., Vaccari, N.E., Waisfeld, B.G., Sánchez, T.M., Foglia, R.D., 2009. Cambrian and Ordovician biogeography of the South American margin of Gondwana and accreted terranes. Early Palaeozoic Peri-Gondwana Terranes: New Insights from Tectonics and Biogeography 325, 201-232. http://dx.doi.org/10.1144/sp325.11

Berger, W.H., Vincent, E., 1981. Chemostratigrapy and biostratigraphic correlation: Exercises in systematic stratigraphy, Proceedings 26th International Geological Congress, Geology of oceans symposium. Oceanologica Acta, Paris, France, pp. 115-127.

Bergström, S.M., Chen, X.U., Gutiérrez-Marco, J.C., Dronov, A., 2009. The new chronostratigraphic classification of the Ordovician System and its relations to major regional series and stages and to $\delta^{13}C$ chemostratigraphy. Lethaia 42, 97-107. http://dx.doi.org/10.1111/j.1502-3931.2008.00136.x

Bowen, G.J., Wilkinson, B., 2002. Spatial distribution of $\delta^{18}O$ in meteoric precipitation. Geology 30, 315-318. http://dx.doi.org/10.1130/0091-7613(2002)030<0315:SDOOIM>2.0.CO;2

Brand, U., Veizer, J., 1980. Chemical diagenesis of a multicomponent carbonate system; 1, Trace elements. Journal of Sedimentary Research 50, 1219-1236. http://dx.doi.org/10.1306/212F7BB7-2B24-11D7-8648000102C1865D

Brenchley, P.J., Marshall, J.D., Carden, G.A.F., Robertson, D.B.R., Long, D.G.F., Meidla, T., Hints, L., Anderson, T.F., 1994. Bathymetric and isotopic evidence for a short-lived Late Ordovician glaciation in a greenhouse period. Geology 22, 295-298. http://dx.doi.org/10.1130/0091-7613(1994)022<0295:baiefa>2.3.co;2

Calner, M., Lehnert, O., Wu, R., Dahlqvist, P., Joachimski, M.M., 2014. $\delta^{13}C$ chemostratigraphy in the Lower–Middle Ordovician succession of Öland (Sweden) and the global significance of the MDICE. GFF 136, 48-54. http://dx.doi.org/10.1080/11035897.2014.901409

Cañas, F.L., 2003. Selected sections of Lower to Middle Ordovician carbonate sedimentation of the Argentine Precordillera: The La Silla and San Juan formations at Cerros La Silla and Niquivil. INSUEGO, Miscelanea 8.

Carpenter, S.J., Lohmann, K.C., 1997. Carbon isotope ratios of Phanerozoic marine cements: Re-evaluating the global carbon and sulfur systems. Geochimica et Cosmochimica Acta 61, 4831-4846. http://dx.doi.org/10.1016/S0016-7037(97)00361-X

Carrera, M.G., 1997. Análisis paleoecológico de la fauna de poríferos del Llanvirniano tardío de la Precordillera Argentina. Ameghiniana 34, 309-316.

Carrera, M.G., Astini, R.A., 1998. Valoracion de las restriciones ambientales durante la transicion Argenigiano-Llanvirniano, Ordovícico de la Precordillera Argentina. Revista de la Asociación Geológica Argentina 53, 41-56.

Cocks, L.R.M., Torsvik, T.H., 2002. Earth geography from 500 to 400 million years ago; a faunal and palaeomagnetic review. Journal of the Geological Society of London 159, Part 6, 631-644. http://dx.doi.org/10.1144/0016-764901-118

Derry, L.A., 2010. A burial diagenesis origin for the Ediacaran Shuram–Wonoka carbon isotope anomaly. Earth and Planetary Science Letters 294, 152-162. http://dx.doi.org/10.1016/j.epsl.2010.03.022

Edwards, C.T., Saltzman, M.R., 2014. Carbon isotope ($\delta^{13}C_{carb}$) stratigraphy of the Lower–Middle Ordovician (Tremadocian–Darriwilian) in the Great Basin, western United States: Implications for global correlation. Palaeogeography, Palaeoclimatology, Palaeoecology 399, 1-20. http://dx.doi.org/10.1016/j.palaeo.2014.02.005

Edwards, C.T., Saltzman, M.R., 2016. Paired carbon isotopic analysis of Ordovician bulk carbonate ($\delta^{13}C_{carb}$) and organic matter ($\delta^{13}C_{org}$) spanning the Great Ordovician

Biodiversification Event. Palaeogeography, Palaeoclimatology, Palaeoecology 458, 102-117. http://dx.doi.org/10.1016/j.palaeo.2015.08.005

England, M.H., 1992. On the Formation of Antarctic Intermediate and Bottom Water in Ocean General Circulation Models. Journal of Physical Oceanography 22, 918-926. http://dx.doi.org/10.1175/1520-0485(1992)022<0918:otfoai>2.0.co;2

Epstein, A.G., Epstein, J.B., Harris, L.D., Geological, S., 1977. Conodont color alteration -- an index to organic metamorphism : experimental and field studies showing the application of conodont color alteration to geothermometry, metamorphism, and structural geology and for assessing hydrocarbon potential. U.S. Govt. Print. Off., Washington.

Fanning, C.M., Pankhurst, R.J., Rapela, C.W., Baldo, E.G., Casquet, C., Galindo, C., 2004. K-bentonites in the Argentine Precordillera contemporaneous with rhyolite volcanism in the Famatinian Arc. Journal of the Geological Society 161, 747-756. http://dx.doi.org/10.1144/0016-764903-130

Feltes, N., Albanesi, G.L., Bergström, S.M., 2016. Conodont biostratigraphy and global correlation of the middle Darriwilian-lower Sandbian (Ordovician) Las Aguaditas Formation, Precordillera of San Juan, Argentina. Andean Geology 43, 60-85. http://dx.doi.org/10.5027/andgeoV43n1-a04

Feltes, N.A., 2017. Fauna de conodontes y graptolitos de la Formación Las Aguaditas (Ordovícico) en el cordón de Los Blanquitos, Precordillera Central de San Juan, Argentina Universidad Nacional de Córdoba, Unpublished Dissertation, p. 453.

Finney, S.C., Berry, W.B.N., Cooper, J.D., Ripperdan, R.L., Sweet, W.C., Jacobson, S.R., Soufiane, A., Achab, A., Noble, P.J., 1999. Late Ordovician mass extinction: A new perspective from stratigraphic sections in central Nevada. Geology 27, 215-218. http://dx.doi.org/10.1130/0091-7613(1999)027<0215:lomean>2.3.co;2

Foster, T.D., Carmack, E.C., 1976. Frontal zone mixing and Antarctic Bottom water formation in the southern Weddell Sea. Deep Sea Research and Oceanographic Abstracts 23, 301-317. http://dx.doi.org/10.1016/0011-7471(76)90872-X

Freeman, K.H., 2001. Isotopic biogeochemistry of marine organic carbon. Reviews in Mineralogy and Geochemistry 43, 579-605. http://dx.doi.org/10.2138/gsrmg.43.1.579

Gilleaudeau, G.J., Kah, L.C., 2013. Carbon isotope records in a Mesoproterozoic epicratonic sea: Carbon cycling in a low-oxygen world. Precambrian Research 228, 85-101. http://dx.doi.org/10.1016/j.precamres.2013.01.006

Guo, H., Du, Y., Kah, L.C., Huang, J., Hu, C., Huang, H., Yu, W., 2013. Isotopic composition of organic and inorganic carbon from the Mesoproterozoic Jixian Group, North China: Implications for biological and oceanic evolution. Precambrian Research 224, 169-183. https://doi.org/10.1016/j.precamres.2012.09.023

Halverson, G.P., Hoffman, P.F., Schrag, D.P., Maloof, A.C., Rice, A.H.N., 2005. Toward a Neoproterozoic composite carbon-isotope record. Geological Society of America Bulletin 117, 1181-1207. http://dx.doi.org/10.1130/b25630.1

Haq, B.U., Schutter, S.R., 2008. A chronology of Paleozoic sea-level changes. Science 322, 64-68. http://dx.doi.org/10.1126/science.1161648

Harper, D.A.T., 2006. The Ordovician biodiversification: Setting an agenda for marine life. Palaeogeography, Palaeoclimatology, Palaeoecology 232, 148-166. http://dx.doi.org/10.1016/j.palaeo.2005.07.010

Harper, D.A.T., Mac Niocaill, C., Williams, S.H., 1996. The palaeogeography of early Ordovician Iapetus terranes: an integration of faunal and palaeomagnetic constraints. Palaeogeography, Palaeoclimatology, Palaeoecology 121, 297-312. http://dx.doi.org/10.1016/0031-0182(95)00079-8

Hayes, J.M., Popp, B.N., Takigiku, R., Johnson, M.W., 1989. An isotopic study of biogeochemical relationships between carbonates and organic carbon in the Greenhorn Formation. Geochimica et Cosmochimica Acta 53, 2961-2972. http://dx.doi.org/10.1016/0016-7037(89)90172-5

Hayes, J.M., Strauss, H., Kaufman, A.J., 1999. The abundance of ^{13}C in marine organic matter and isotopic fractionation in the global biogeochemical cycle of carbon during the past 800 Ma. Chemical Geology 161, 103-125. http://dx.doi.org/10.1016/S0009-2541(99)00083-2

Heredia, S., Beresi, M., Peralta, S., 2005. Darriwilian conodont biostratigraphy of the Las Chacritas Formation, Central Precordillera (San Juan Province, Argentina). Geologica Acta 3, 385-394.

Holmden, C., Creaser, R.A., Muehlenbachs, K., Leslie, S.A., Bergström, S.M., 1998. Isotopic evidence for geochemical decoupling between ancient epeiric seas and bordering oceans: Implications for secular curves. Geology 26, 567-570. http://dx.doi.org/10.1130/0091-7613(1998)026<0567:iefgdb>2.3.co;2

Huff, W., Davis, D., Bergström, S., Krekeler, M., Kolata, D., Cingolani, C., 1997. A biostratigraphically well-constrained K-bentonite U-Pb zircon age of the lowermost Darriwilian Stage (Middle Ordovician) from the Argentine Precordillera. Episodes 20, 29-33. https://doi.org/10.1144/0016-764903-130

Huff, W.D., Bergström, S.M., Kolata, D.R., Cingolani, C., Davis, D.W., 1995. Middle Ordovician K-bentonites discovered in the Precordillera of Argentina: Geochemical and paleogeographical implications, in: Cooper, J.D., Droser, M.L., Finney, S.C. (Eds.), Ordovician oddesy: Short papers for the Seventh International Symposium on the Ordovician System. The Pacific Section Society for Sedimentary Geology 77, 343-349.

Huff, W.D., Bergström, S.M., Kolata, D.R., Cingolani, C.A., Astini, R.A., 1998. Ordovician K-bentonites in the Argentine Precordillera: relations to Gondwana margin evolution. Geological Society, London, Special Publications 142, 107-126. 10.1144/gsl.sp.1998.142.01.06

Jaffrés, J.B.D., Shields, G.A., Wallmann, K., 2007. The oxygen isotope evolution of seawater: A critical review of a long-standing controversy and an improved geological water cycle model for the past 3.4 billion years. Earth-Science Reviews 83, 83-122. http://dx.doi.org/10.1016/j.earscirev.2007.04.002

Jahren, A.H., Porter, S., Kuglitsch, J.J., 2003. Lichen metabolism identified in Early Devonian terrestrial organisms. Geology 31, 99-102. 10.1130/0091-7613(2003)031<0099:lmiied>2.0.co;2

Kah, L.C., Bartley, J.K., Teal, D.A., 2012. Chemostratigraphy of the Late Mesoproterozoic Atar Group, Taoudeni Basin, Mauritania: Muted isotopic variability, facies correlation, and global isotopic trends. Precambrian Research 200–203, 82-103. http://dx.doi.org/10.1016/j.precamres.2012.01.011

Kah, L.C., Sherman, A.G., Narbonne, G.M., Knoll, A.H., Kaufman, A.J., 1999. $\delta^{13}C$ stratigraphy of the Proterozoic Bylot Supergroup, Baffin Island, Canada: implications for regional lithostratigraphic correlations. Canadian Journal of Earth Sciences 36, 313-332. http://dx.doi.org/10.1139/e98-100

Kah, L.C., Thompson, C.K., Henderson, M.A., Zhan, R., 2016. Behavior of marine sulfur in the Ordovician. Palaeogeography, Palaeoclimatology, Palaeoecology 458, 133-153. http://dx.doi.org/10.1016/j.palaeo.2015.12.028

Kaljo, D., Martma, T., Saadre, T., 2007. Post-Hunnebergian Ordovician carbon isotope trend in Baltoscandia, its environmental implications and some similarities with that of Nevada. Palaeogeography, Palaeoclimatology, Palaeoecology 245, 138-155. http://dx.doi.org/10.1016/j.palaeo.2006.02.020

Kaufman, A.J., Hayes, J.M., Knoll, A.H., Germs, G.J.B., 1991. Isotopic compositions of carbonates and organic carbon from upper Proterozoic successions in Namibia: stratigraphic variation and the effects of diagenesis and metamorphism. Precambrian Research 49, 301-327. http://dx.doi.org/10.1016/0301-9268(91)90039-D

Kaufman, A.J., Knoll, A.H., 1995. Neoproterozoic variations in the C-isotopic composition of seawater: stratigraphic and biogeochemical implications. Precambrian Research 73, 27-49. http://dx.doi.org/10.1016/0301-9268(94)00070-8

Keller, M., 1999. Argentine Precordillera: Sedimentary and plate tectonic history of a Laurentian crustal fragment in South America. Geological Society of America Special Paper 341. https://dx.doi.org/10.1130/0-8137-2341-8.1

Keller, M., Eberlein, S., Lehnert, O., 1993. Sedimentology of middle ordovician carbonates in the Argentine precordillera: evidence of regional relative sea-level changes. Geol Rundsch 82, 362-377. http://dx.doi.org/10.1007/BF00191838

Knauth, L.P., Kennedy, M.J., 2009. The late Precambrian greening of the Earth. Nature 460, 728-732. http://dx.doi.org/doi:10.1038/nature08213

Knoll, A.H., Bambach, R.K., Canfield, D.E., Grotzinger, J.P., 1996. Comparative Earth History and Late Permian Mass Extinction. Science 273, 452-457. 10.1126/science.273.5274.452

Kolata, D.R., Huff, W.D., Bergström, S.M., 2001. The Ordovician Sebree Trough: An oceanic passage to the Midcontinent United States. GSA Bulletin 113, 1067-1078. http://dx.doi.org/10.1130/0016-7606(2001)113<1067:TOSTAO>2.0.CO;2

Küspert, W., 1982. Environmental Changes During Oil Shale Deposition as Deduced from Stable Isotope Ratios, in: Einsele, G., Seilacher, A. (Eds.), Cyclic and Event Stratification. Springer Berlin Heidelberg, Berlin, Heidelberg, pp. 482-501. 10.1007/978-3-642-75829-4_36

Leslie, S.A., Saltzman, M.R., Bergström, S.M., Repetski, J.E., Howard, A., Seward, A.M., 2011. Conodont biostratigraphy and stable isotope stratigraphy across the Ordovician Knox/Beekmantown unconformity in the central Appalachians, in: Gutiérrez-Alonso, G.,

Diego, G.B. (Eds.), Ordovician of the World. Publicaciones del Instituto Geológico y Minero de España.

Löfgren, A., Tolmacheva, T., 2008. Morphology, evolution and stratigraphic distribution in the Middle Ordovician conodont genus *Microzarkodina*. Earth and Environmental Science Transactions of the Royal Society of Edinburgh 99, 27-48. 10.1017/S1755691008007056

Lohmann, K.C., 1988. Geochemical Patterns of Meteoric Diagenetic Systems and Their Application to Studies of Paleokarst, in: James, N.P., Choquette, P.W. (Eds.), Paleokarst. Springer New York, New York, NY, pp. 58-80. http://dx.doi.org/10.1007/978-1-4612-3748-8_3

Marenco, P.J., Marenco, K.N., Lubitz, R.L., Niu, D., 2013. Contrasting long-term global and short-term local redox proxies during the Great Ordovician Biodiversification Event: A case study from Fossil Mountain, Utah, USA. Palaeogeography, Palaeoclimatology, Palaeoecology 377, 45-51. http://dx.doi.org/10.1016/j.palaeo.2013.03.007

Marshall, J.D., 1992. Climatic and oceanographic isotopic signals from the carbonate rock record and their preservation. Geological Magazine 129, 143-160. https://doi.org/10.1017/S0016756800008244

Martma, T., 2005. Ordovician carbon isotopes, in: Põldvere, A. (Ed.), Mehikoorma (421) Drill Core: Estonian Geological Sections. Estonian Geological Survey Bulletin, pp. 25-27.

Meidla, T., Backman, L., Dronov, A., Holmer, L., Sturesson, U., 2004. Middle-Upper Ordovician carbon isotope record from Västergötland (Sweden) and East Baltic, in:

Hints, O., Ainsaar, L. (Eds.), 8th Meeting on the Working Group on the Ordovician Geology of Baltoscandia. Tartu University Press, Tallinn and Tartu, Estonia, pp. 67-68.

Panchuk, K.M., Holmden, C.E., Leslie, S.A., 2006. Local controls on carbon cycling in the Ordovician midcontinent region of North America, with implications for carbon isotope secular curves. Journal of Sedimentary Research 76, 200-211. http://dx.doi.org/10.2110/jsr.2006.017

Pankhurst, R.J., Rapela, C.W., Fanning, C.M., 2000. Age and origin of coeval TTG, I- and S-type granites in the Famatinian belt of NW Argentina. Geological Society of America Special Papers 350, 151-168. http://dx.doi.org/10.1130/0-8137-2350-7.151

Patterson, W.P., Walter, L.M., 1994. Depletion of ^{13}C in seawater ΣCO_2 on modern carbonate platforms: Significance for the carbon isotopic record of carbonates. Geology 22, 885-888. http://dx.doi.org/10.1130/0091-7613(1994)022<0885:docisc>2.3.co;2

Peralta, G.L., Baldis, B.A.J., 1995. Graptolites y trilobites del Ordovícico tardío en el perfil del río de Las Chacritas, Precordillera Central de San Juan, Argentina. V Congreso Argentino Paleontología y Bioestratigrafía, Trelew (1994), Actas, 201-205.

Peralta, S.H., Heredia, S., Beresi, M.S., 1999. Upper Arenigian-lower Llanvirnian sequence of the Las Chacritas river, Central Precordillera, San Juan Province, Argentina. Acta Universitatis Carolinae Geologica 43, 123-126.

Pope, M.C., Steffen, J.B., 2003. Widespread, prolonged late Middle to Late Ordovician upwelling in North America: A proxy record of glaciation? Geology 31, 63-66. http://dx.doi.org/10.1130/0091-7613(2003)031<0063:wplmtl>2.0.co;2

Railsback, L.B., Ackerly, S.C., Anderson, T.F., Cisneti, J.L., 1990. Palaeontological and isotope evidence for warm saline deep waters in Ordovician oceans. Nature 343, 156-159. http://dx.doi.org/10.1038/343156a0

Railsback, L.B., Holland, S.M., Hunter, D.M., Jordan, E.M., Díaz, J.R., Crowe, D.E., 2003. Controls on Geochemical Expression of Subaerial Exposure in Ordovician Limestones from the Nashville Dome, Tennessee, U.S.A. Journal of Sedimentary Research 73, 790-805. http://dx.doi.org/10.1306/020503730790

Ramos, V.A., Jordan, T.E., Allmendinger, R.W., Mpodozis, C., Kay, S.M., Cortes, J.M., Palma, M., 1986. Paleozoic terranes of the Central Argentine-Chilean Andes. Tectonics 5, 855-880. http://dx.doi.org/10.1029/TC005i006p00855

Rasmussen, C.M.Ø., Ullmann, C.V., Jakobsen, K.G., Lindskog, A., Hansen, J., Hansen, T., Eriksson, M.E., Dronov, A., Frei, R., Korte, C., Nielsen, A.T., Harper, D.A.T., 2016. Onset of main Phanerozoic marine radiation sparked by emerging Mid Ordovician icehouse. Scientific Reports 6, 18884. http://dx.doi.org/10.1038/srep18884

Saltzman, M.R., 2005. Phosphorus, nitrogen, and the redox evolution of the Paleozoic oceans. Geology 33, 573-576. http://dx.doi.org/10.1130/g21535.1

Saltzman, M.R., Edwards, C.T., 2017. Gradients in the carbon isotopic composition of Ordovician shallow water carbonates: A potential pitfall in estimates of ancient CO_2 and O_2. Earth and Planetary Science Letters 464, 46-54. http://dx.doi.org/10.1016/j.epsl.2017.02.011

Saltzman, M.R., Runnegar, B., Lohmann, K.C., 1998. Carbon isotope stratigraphy of Upper Cambrian (Steptoean Stage) sequences of the eastern Great Basin: Record of a global oceanographic event. Geological Society of America Bulletin 110, 285-297. http://dx.doi.org/10.1130/0016-7606(1998)110<0285:cisouc>2.3.co;2

Saltzman, M.R., Thomas, E., 2012. Carbon isotope stratigraphy, in: Gradstein, F.M., Ogg, J., Schmitz, M.D., Ogg, G. (Eds.), The Geologic Time Scale, 1 ed. Elsevier, pp. 207-232. http://dx.doi.org/10.1016/B978-0-444-59425-9.00011-1

Saltzman, M.R., Young, S.A., 2005. Long-lived glaciation in the Late Ordovician? Isotopic and sequence-stratigraphic evidence from western Laurentia. Geology 33, 109-112. http://dx.doi.org/10.1130/g21219.1

Sarkar, S., Chakraborty, P.P., Bhattacharya, S.K., Banerjee, S., 1998. C^{12}-enrichment along intraformational unconformities within Proterozoic Bhander Limestone, Son valley, India and its implication. Carbonates and Evaporites 13, 108. http://dx.doi.org/10.1007/bf03175440

Schmitz, B., Bergström, S.M., Xiaofeng, W., 2010. The middle Darriwilian (Ordovician) $\delta^{13}C$ excursion (MDICE) discovered in the Yangtze Platform succession in China: implications of its first recorded occurrences outside Baltoscandia. Journal of the Geological Society 167, 249-259. http://dx.doi.org/10.1144/0016-76492009-080

Scholle, P.A., Ulmer-Scholle, D.S., 2003. Color guide to the Petrography of Carbonate Rocks, 2 ed.

Schrag, D.P., Higgins, J.A., Macdonald, F.A., Johnston, D.T., 2013. Authigenic Carbonate and the History of the Global Carbon Cycle. Science 339, 540-543. http://dx.doi.org/10.1126/science.1229578

Serra, F., Albanesi, G.L., Ortega, G., Bergström, S.M., 2015. Biostratigraphy and palaeoecology of Middle–Late Ordovician conodont and graptolite faunas of the Las Chacritas River section, Precordillera of San Juan, Argentina. Geological Magazine 152, 813-829. http://dx.doi.org/10.1017/S0016756814000752

Serra, F., Feltes, N.A., Henderson, M.A., Albanesi, G.L., 2017. Darriwilian (Middle Ordovician) conodont biofacies from the Central Precordillera of Argentina. Marine Micropaleontology 130, 15-28. http://dx.doi.org/10.1016/j.marmicro.2016.12.002

Servais, T., Danelian, T., Harper, D.A.T., Munnecke, A., 2014. Possible oceanic circulation patterns, surface water currents and upwelling zones in the Early Palaeozoic. Gff 136, 229-233. http://dx.doi.org/10.1080/11035897.2013.876659

Servais, T., Owen, A.W., Harper, D.A.T., Kröger, B., Munnecke, A., 2010. The Great Ordovician Biodiversification Event (GOBE): The palaeoecological dimension. Palaeogeography, Palaeoclimatology, Palaeoecology 294, 99-119. http://dx.doi.org/10.1016/j.palaeo.2010.05.031

Spero, H.J., Bijma, J., Lea, D.W., Bemis, B.E., 1997. Effect of seawater carbonate concentration on foraminiferal carbon and oxygen isotopes. Nature 390, 497-500.

Stouge, S., 2012. Middle Ordovician (late Dapingian–Darriwilian) conodonts from the Cow Head Group and Lower Head Formation, western Newfoundland, Canada, CJES Special

Issue: In honour of Ward Neale on the theme of Appalachian and Grenvillian geology. Canadian Journal of Earth Sciences 49, 59-90. 10.1139/e11-057

Stouge, S.S., 1984. Conodonts of the Middle Ordovician Table Head Formation, western Newfoundland. Lethaia: Fossils and Strata 16, 1-149.

Strother, P.K., Al-Hajri, S., Traverse, A., 1996. New evidence for land plants from the lower Middle Ordovician of Saudi Arabia. Geology 24, 55-58. 10.1130/0091-7613(1996)024<0055:NEFLPF>2.3.CO;2

Thamdrup, B., Rosselló-Mora, R., Amann, R., 2000. Microbial manganese and sulfate reduction in Black Sea shelf sediments. Applied and Environmental Microbiology 66, 2888-2897. http://dx.doi.org/10.1128/aem.66.7.2888-2897.2000

Thomas, W.A., 2011. The Iapetan rifted margin of southern Laurentia. Geosphere 7, 97-120. http://dx.doi.org/10.1130/ges00574.1

Thomas, W.A., Astini, R.A., 1996. The Argentine Precordillera: A traveler from the Ouachita embayment of North American Laurentia. Science 273, 752-757. http://dx.doi.org/10.1126/science.273.5276.752

Thomas, W.A., Astini, R.A., Bayona, G., 2002. Ordovician collision of the Argentine Precordillera with Gondwana, independent of Laurentian Taconic orogeny. Tectonophysics 345, 131-152. http://dx.doi.org/10.1016/S0040-1951(01)00210-4

Thomas, W.A., Astini, R.A., Denison, R.E., 2001. Strontium isotopes, age, and tectonic setting of Cambrian salinas along the rift and transform margins of the Argentine Precordillera and southern Laurentia. Journal of Geology 109, 231-246. http://dx.doi.org/10.1086/319241

Thompson, C.K., Kah, L.C., 2012. Sulfur isotope evidence for widespread euxinia and a fluctuating oxycline in Early to Middle Ordovician greenhouse oceans. Palaeogeography, Palaeoclimatology, Palaeoecology 313-314, 189-214. http://dx.doi.org/10.1016/j.palaeo.2011.10.020

Thompson, C.K., Kah, L.C., Astini, R., Bowring, S.A., Buchwaldt, R., 2012. Bentonite geochronology, marine geochemistry, and the Great Ordovician Biodiversification Event (GOBE). Palaeogeography, Palaeoclimatology, Palaeoecology 321–322, 88-101. http://dx.doi.org/10.1016/j.palaeo.2012.01.022

Trotter, J.A., Williams, I.S., Barnes, C.R., Lécuyer, C., Nicoll, R.S., 2008. Did Cooling Oceans Trigger Ordovician Biodiversification? Evidence from Conodont Thermometry. Science 321, 550-554. http://dx.doi.org/10.1126/science.1155814

Van Cappellen, P., Ingall, E.D., 1994. Benthic phosphorus regeneration, net primary production, and ocean anoxia: A model of the coupled marine biogeochemical cycles of carbon and phosphorus. Paleoceanography 9, 677-692. http://dx.doi.org/10.1029/94PA01455

Veizer, J., 1983. Chemical diagenesis of carbonates; therory and application of trace element technique, in: Arthur, M.A., Anderson, T.F., Kaplan, I.R., Veizer, J., Land, L.S. (Eds.), Stable isotopes in sedimentary geology. Society of Sedimentary Geology, Tulsa, OK, SEPM Short Course (1983).

Veizer, J., Ala, D., Azmy, K., Bruckschen, P., Buhl, D., Bruhn, F., Carden, G.A.F., Diener, A., Ebneth, S., Godderis, Y., Jasper, T., Korte, C., Pawellek, F., Podlaha, O.G., Strauss, H.,

1999. $^{87}Sr/^{86}Sr$, $\delta^{13}C$ and $\delta^{18}O$ evolution of Phanerozoic seawater. Chemical Geology 161, 59-88. http://dx.doi.org/10.1016/S0009-2541(99)00081-9

Viira, V., 2011. Lower and Middle Ordovician conodonts from the subsurface of SE Estonia and adjacent Russia. Estonian Journal of Earth Sciences 60, 1-21. http://dx.doi.org/10.3176/earth.2011.1.01

von Gosen, W., 1997. Early Paleozoic and Andean structural evolution in the Rio Jáchal section of the Argentine Precordillera. Journal of South American Earth Sciences 10, 361-388. http://dx.doi.org/10.1016/S0895-9811(97)00029-1

Webby, B.D., Droser, M.L., Paris, F., and Percival, I., 2004. The Great Ordovician Biodiversification Event, in: Webby, B.D., Droser, M.L., Paris, F., and Percival, I. (Ed.), The Great Ordovician Biodviersification Event. Columbia University Press, New York, p. 484. http://dx.doi.org/10.1017/S0016756805220782

Young, S.A., Gill, B.C., Edwards, C.T., Saltzman, M.R., Leslie, S.A., 2016. Middle–Late Ordovician (Darriwilian–Sandbian) decoupling of global sulfur and carbon cycles: Isotopic evidence from eastern and southern Laurentia. Palaeogeography, Palaeoclimatology, Palaeoecology 458, 118-132. http://dx.doi.org/10.1016/j.palaeo.2015.09.040

Zapata, T.R., Allmendinger, R.W., 1996. Thrust-front zone of the Precordillera, Argentina: A thick-skinned triangle zone. Aapg Bulletin-American Association of Petroleum Geologists 80, 359-381.

Zhang, J., Quay, P.D., Wilbur, D.O., 1995. Carbon isotope fractionation during gas-water exchange and dissolution of CO_2. Geochimica et Cosmochimica Acta 59, 107-114. http://dx.doi.org/10.1016/0016-7037(95)91550-D

Zhang, J.H., 1998. Conodonts from the Guniutan Formation (Llanvirnian) in Hubei and Hunan Provinces, south-central China. Almqvist and Wiksell International.

Zhang, T., Shen, Y., Algeo, T.J., 2010. High-resolution carbon isotopic records from the Ordovician of South China: Links to climatic cooling and the Great Ordovician Biodiversification Event (GOBE). Palaeogeography, Palaeoclimatology, Palaeoecology 289, 102-112. http://dx.doi.org/10.1016/j.palaeo.2010.02.020

Figure captions:

Figure 1. Paleogeographic reconstruction for the Middle Ordovician (~ 470 Ma) after Cocks and Torsvik (2002). Major landmasses are depicted in white, and peri-Gondwanan terranes are depicted in shades of gray. The Precordilleran terrane is shown in dark gray, in a position close to Gondwana, prior to its final docking.

Figure 2. Regional map of the Argentine Precordillera modified from Gomez and Astini (2015). Lower Paleozoic strata crop out in a series of N-S trending thrust sheets and are divided into the Western and Eastern tectofacies. The Western tectofacies consists predominately of metamorphosed and deformed deep-water shale facies. The Eastern tectofacies consists of weakly deformed and unmetamorphosed marine shelf and slope deposits. Coeval measured sections of the Las Chacritas (C) and Las Aguaditas (A) formations were sampled in the Eastern tectofacies to the southwest of San Jose de Jáchal.

Figure 3. Biostratigraphic chart of Darriwilian strata showing generalized conodont zones for the Argentine Precordillera, specific data from the Las Chacritas and Las Aguaditas formations, and summary of data from Scandinavia, the North Atlantic, and China. Data is compiled from Albanesi and Ortega (2016), Serra et al. (2015), Feltes et al. (2016), Zhang (1998) and Löfgren and Tomacheva (2008), Stouge (1984), and Zhang (1998). Stage slices are after Bergström et al. (2009) and time slices after Webby et al. (2004). Interval of interest is indicated in light gray.

Figure 4. Correlation of measured stratigraphic sections of the Las Chacritas and Las Aguaditas formations based on conodont biostratigraphic analysis of Serra et al. (2015) and Feltes et al.

(2016). Upper Darriwilian (Dw3) strata in the Precordillera is absent and inferred to have been removed during development of a regional unconformity. Absence of the Upper Darriwilian is identified by the absence of conodonts representing the upper *E. suecicus* Zone and *P. serra* Zone in the Las Chacritas Formation, and the *E. suecicus* and *P. serra* zones in the Las Aguaditas Formation.

Figure 5. Petrographic microfabrics from the Las Chacritas Formation. A) Fossiliferous packstone with abundant sponge spicules, gastropods, and fragments of bryozoans, trilobites, brachiopods, and echinoderms. B) Intramicrite showing micritic clasts within a micritic- to microsparitic-matrix. Disseminated pyrite (opaque) occurs within the microsparitic matrix. C) Fossiliferous packstone with trilobite fragments, echinoderm fragments, and recrystallized sponge spicules. D) Carbonate mudstone containing predominantly recrystallized sponge spicules. E) CL image of heterogeneous, dully luminescent matrix cut by vein of brightly luminescent calcite with dully luminescent calcite intergrowths. F) CL image of heterogeneously luminescent carbonate matrix with two distinct vein generations: a dully luminescent vein (~ 140 μm diameter) and moderately luminescent vein (> 1 mm diameter).

Figure 6. Petrographic microfabrics from the Las Aguaditas Creek Formation. A) Fossiliferous packstone with abundant fragments of bryozoans, echinoderms, brachiopods, and trilobites, here cut by a large (1 mm diameter) calcite vein and a smaller (~ 15 μm diameter) calcite vein. B) Homogeneous mixture of micritic to microsparitic carbonate and clay; such fabric characterizes the majority of the Las Aguaditas Formation. C) Homogeneous silty carbonate with disseminated pyrite. D) Laminated carbonate mudstone with a single layer of skeletal fragments within a

microsparitic matrix. The white arrow indicates the position of a trilobite fragment. E). CL image showing heterogeneously luminescent micritic matrix composed of dully luminescent micrtitic clasts within a matrix of micrite (mixed luminescence) and clay (non-luminescent), cut by a coarsely crystalline, moderately luminescent vein. F) CL image of heterogeneous carbonate mudstone with three distinct stages of veins mineralization.

Figure 7. Cross-plot of carbon and oxygen isotopes from the Las Chacritas (LCF) and Las Aguaditas (LAF) formations. No clear covariant trends occur between C and O for the various carbonate phases (i.e., microsparitic matrix, recrystallized sparry patches within otherwise micritic matrix, and late-stage mineralized veins). Oxygen isotope compositions of micritic carbonate in the Las Chacritas and Las Aguaditas formations are similar, ranging from −4 ‰ to −6 ‰ in the Las Chacritas Formation and from −4 ‰ to −7 ‰ in the Las Aguaditas Formation. Carbon isotope compositions in both formations range from approximately +1 to −2 ‰. Isotopic compositions of sparry calcite within the carbonate matrix is generally similar to that of matrix micrite, consistent with only minor recrystallization either in the original depositional environment, or within a rock-buffered system. The wide range of $\delta^{18}O$ compositions preserved in vein calcite is consistent with formation by later diagenetic fluids that did not interact substantially with matrix components.

Figure 8. Isotopic and elemental data for carbonate phases of the Las Chacritas Formation. A) Detail of Figure 7; mineralized veins record a unique trajectory in carbon-oxygen space, indicating little influence of late-stage fluids on matrix components. B) Strontium concentrations of matrix components range from approximately 250 to 2000 ppm, consistent with well-

preserved marine limestone. Lower Sr concentrations within sparry matrix is consistent with Sr loss during recrystallization. C) Mn and Fe concentrations are generally elevated, with [Mn] >500 ppm, and [Fe] as high as 8000 ppm. Combined with elevated Sr concentrations that suggest limited recrystallization, elevated Mn and Fe values potentially reflect in-situ incorporation from dysoxic to anoxic marine waters or pore fluids. D) Mn/Sr ratios are generally less than 3, well below the established threshold for little-altered carbonate rocks (Mn/Sr >10; Kaufman et al. 1995).

Figure 9. Isotopic and elemental data for carbonate phases of the Las Aguaditas Formation. A) Detail of Figure 7; mineralized veins record a unique trajectory in carbon-oxygen space, indicating little influence of late-stage fluids on matrix components. B) Elevated Sr concentrations observed in the Las Aguaditas Formation are consistent with crystallization from seawater or recrystallization in the presence of seawater derived fluids during early diagenesis. C) Evidence for elevated Mn and Fe, in conjunction with elevated Sr concentrations, is consistent with Mn and Fe enrichment in primary and early diagenetic fluids. D) Despite a few Mn/Sr values as high as 6.66, Mn/Sr ratios are generally less than 1, well below the established threshold for little-altered carbonate rocks (Mn/Sr >10; Kaufman et al. 1995).

Figure 10. C-isotope records from the Las Chacritas and Las Aguaditas formations. Chemostratigraphic profiles show $\delta^{13}C_{carb}$ compositions are consistently near −1 ‰ through the *Y. crassus* conodont zone. In the Las Chacritas Formation, $\delta^{13}C_{carb}$ values increase from approximately −1.0 ‰ in the lower *E. pseudoplanus* Zone to greater than +1.0 ‰ in the *E. suecicus* Zone. This nearly 2 ‰ positive shift in $\delta^{13}C_{carb}$ values is consistent with the initiation of

the MDICE. In time-equivalent strata of the Las Aguaditas Formation, however, $\delta^{13}C_{carb}$ values abruptly decline to approximately −1.5 ‰. Inferred trends indicated with gray boxes. Three-point moving averages are fit to $\delta^{13}C_{carb}$ profiles.

Figure 11. C-isotope records from the Las Chacritas and Las Aguaditas formations. Organic C-isotopes record substantial variation between −25 ‰ and −30 ‰, although most values are near −28 ‰. C-isotope values within the deeper-water Las Aguaditas Formation are similarly volatile, yet show an abrupt transition to values near −30 ‰ at the transition between the Las Aguaditas Formation and the underlying San Juan Formation. Differences in isotopic composition between the two sections potentially reflect local control on the isotopic composition of DIC. Three-point moving averages are fit to $\delta^{13}C_{org}$ profiles.

Figure 12. Interpretation of the marine shelf of the Las Chacritas and Las Aguaditas formations. Sedimentological data suggests that the Las Chacritas Formation (C) represents depositional environments between fair-weather and storm wave base, whereas sedimentary features of the Las Aguaditas Formation (A) suggest deposition at or near storm wave base. We suggest that the presence of a persistent marine chemocline (cf. Thompson and Kah, 2012) can best explain $\delta^{13}C_{carb}$ and $\delta^{13}C_{org}$ profiles of Figure 10. When carbonate formation occurs above the marine chemocline, marine carbonate reflects the isotopic composition of DIC within well-mixed oxygenated waters. By contrast, deposition below the marine chemocline may contain a mix of allochthonous and autochthonous components (C') and (A'). Carbon isotope compositions of autochthonous carbonate reflect a mixture of marine DIC and DIC from the remineralization of organic matter. Similarly, carbon isotope compositions of autochthonous organic matter

potentially reflect a combination of photosynthetic and heterotrophic metabolisms, resulting in isotopically depleted signatures.

Figure 1

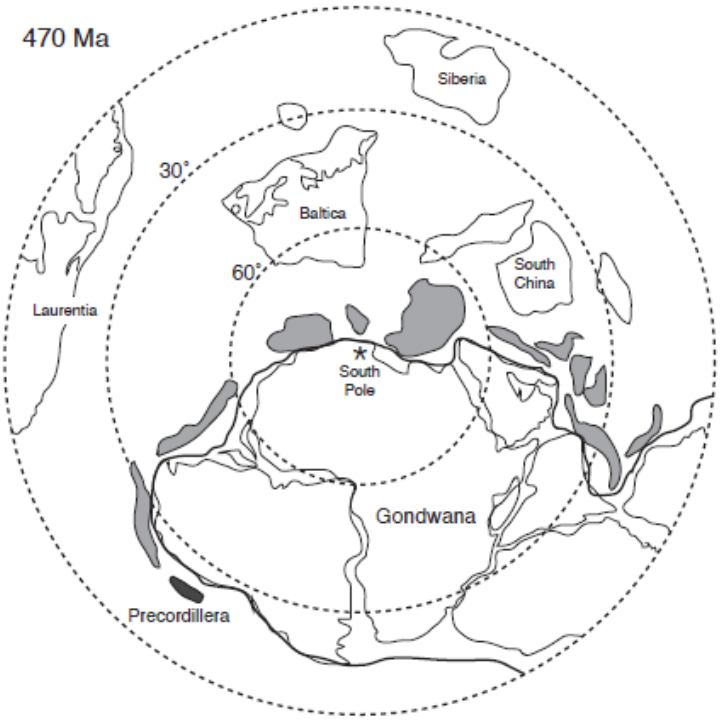

Figure 2

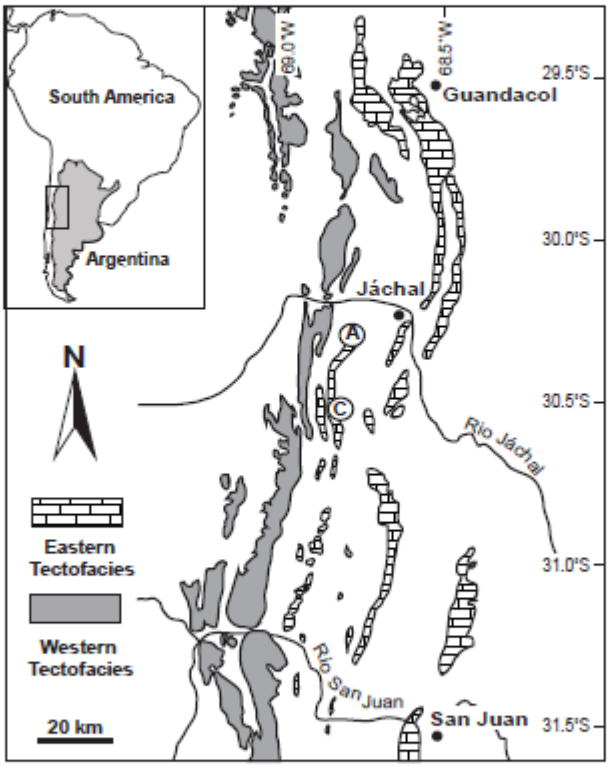

Figure 3

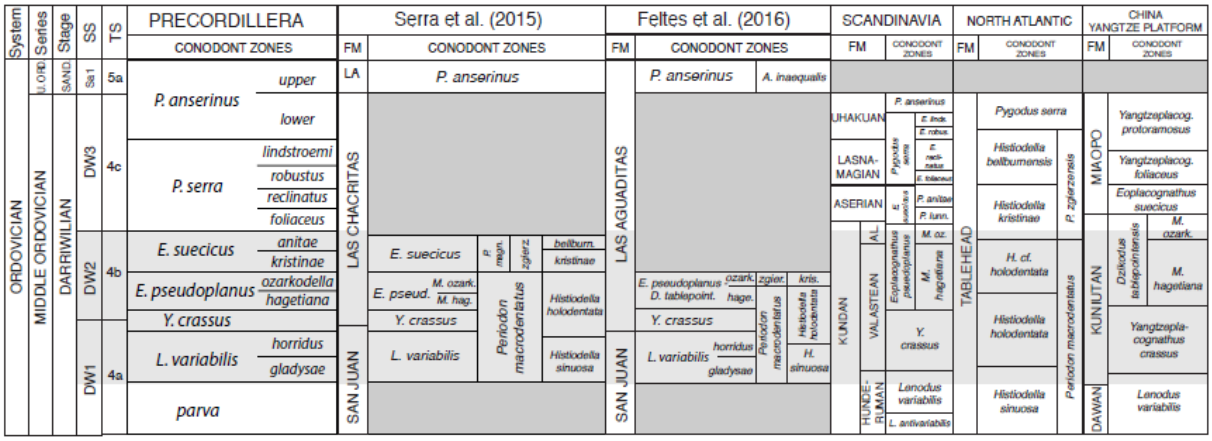

Figure 4

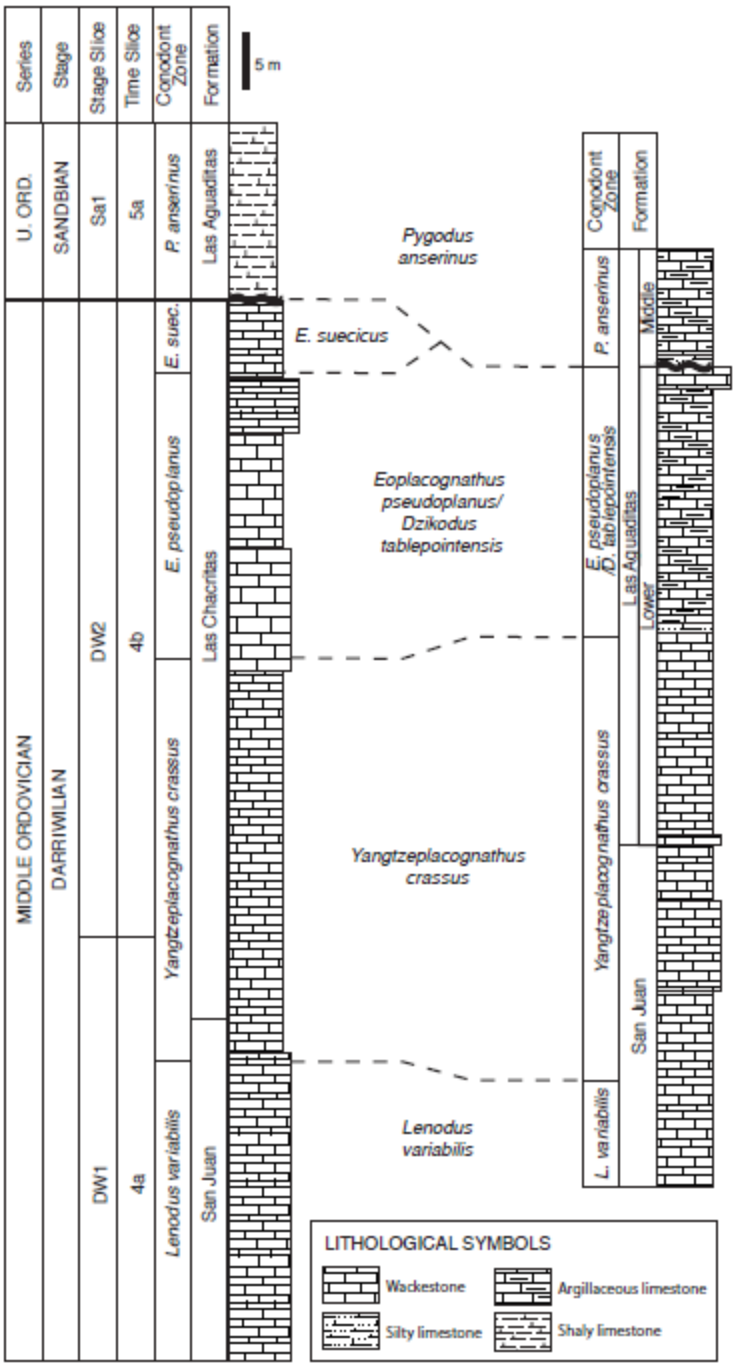

Figure 5

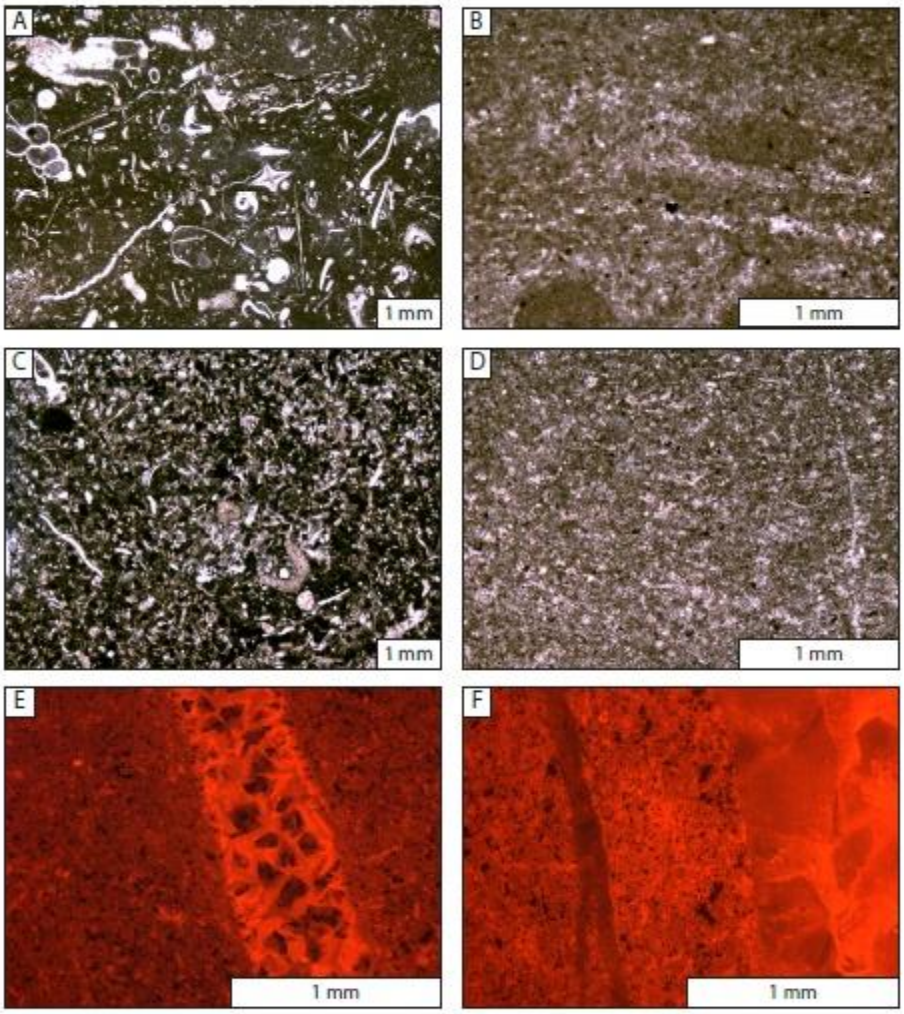

Figure 6

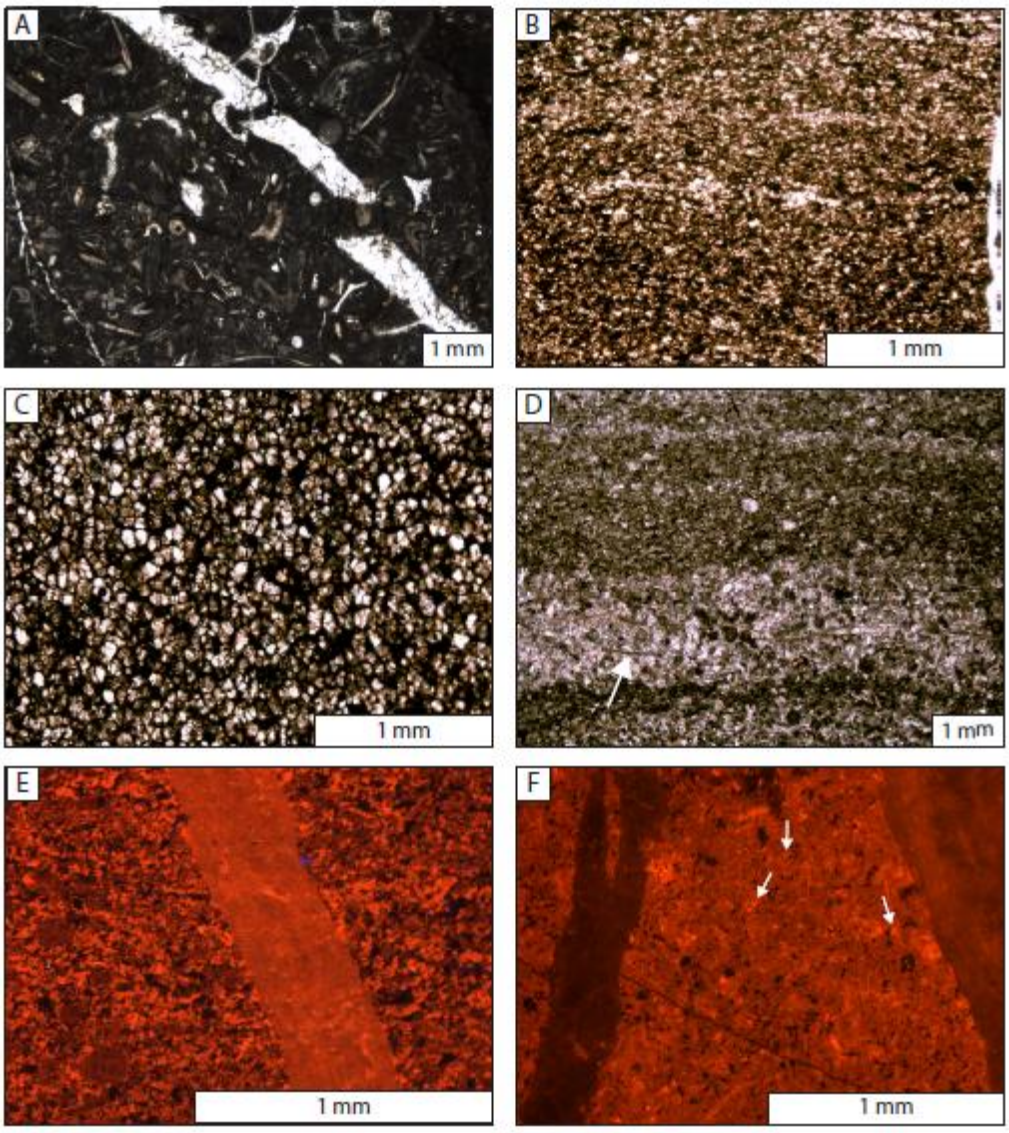

Figure 7

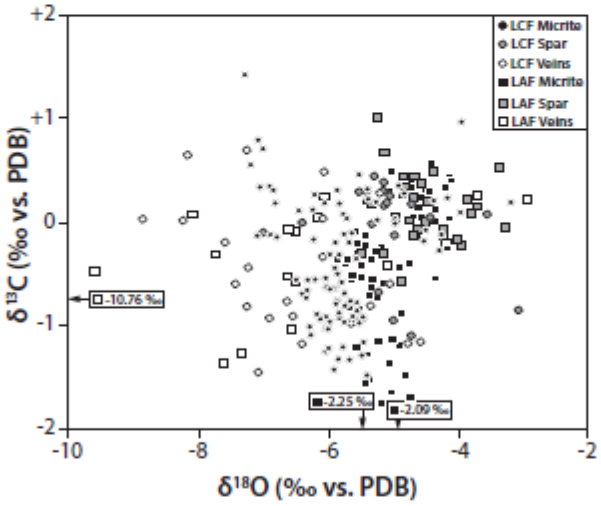

Figure 8

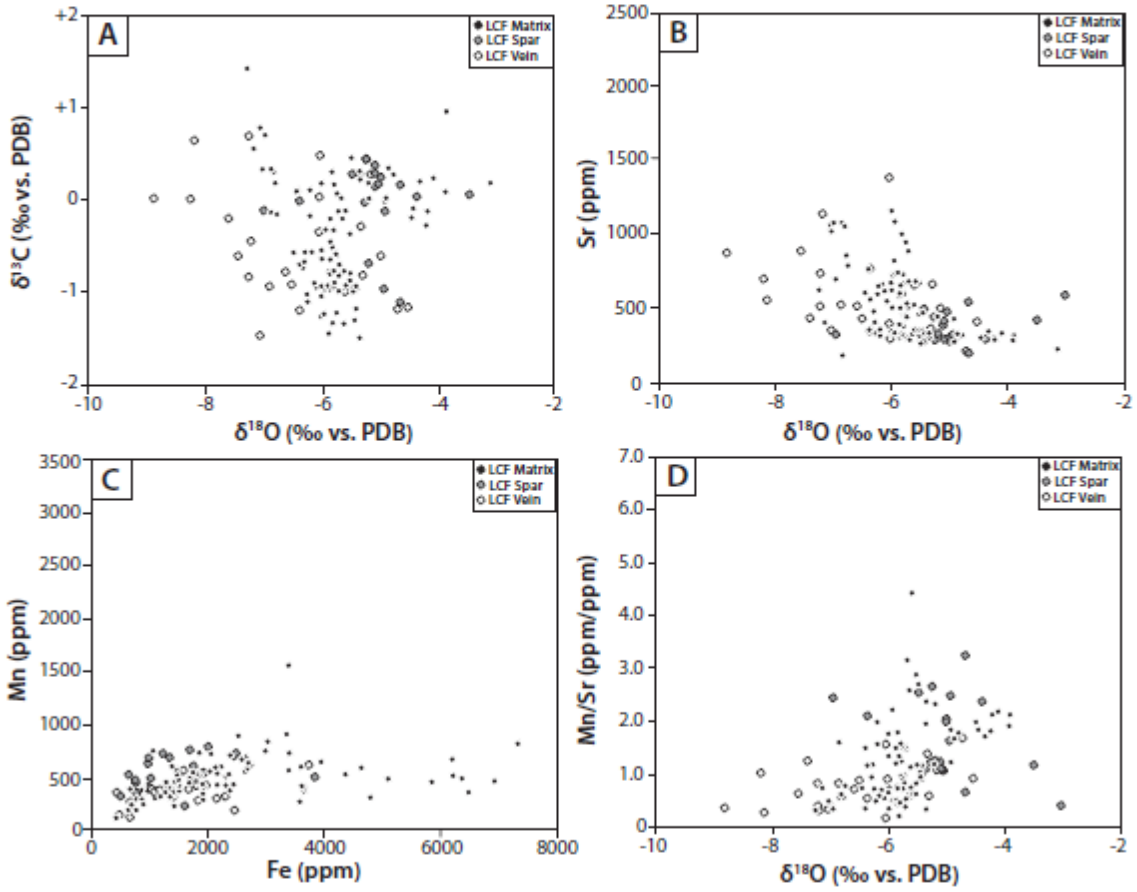

Figure 9

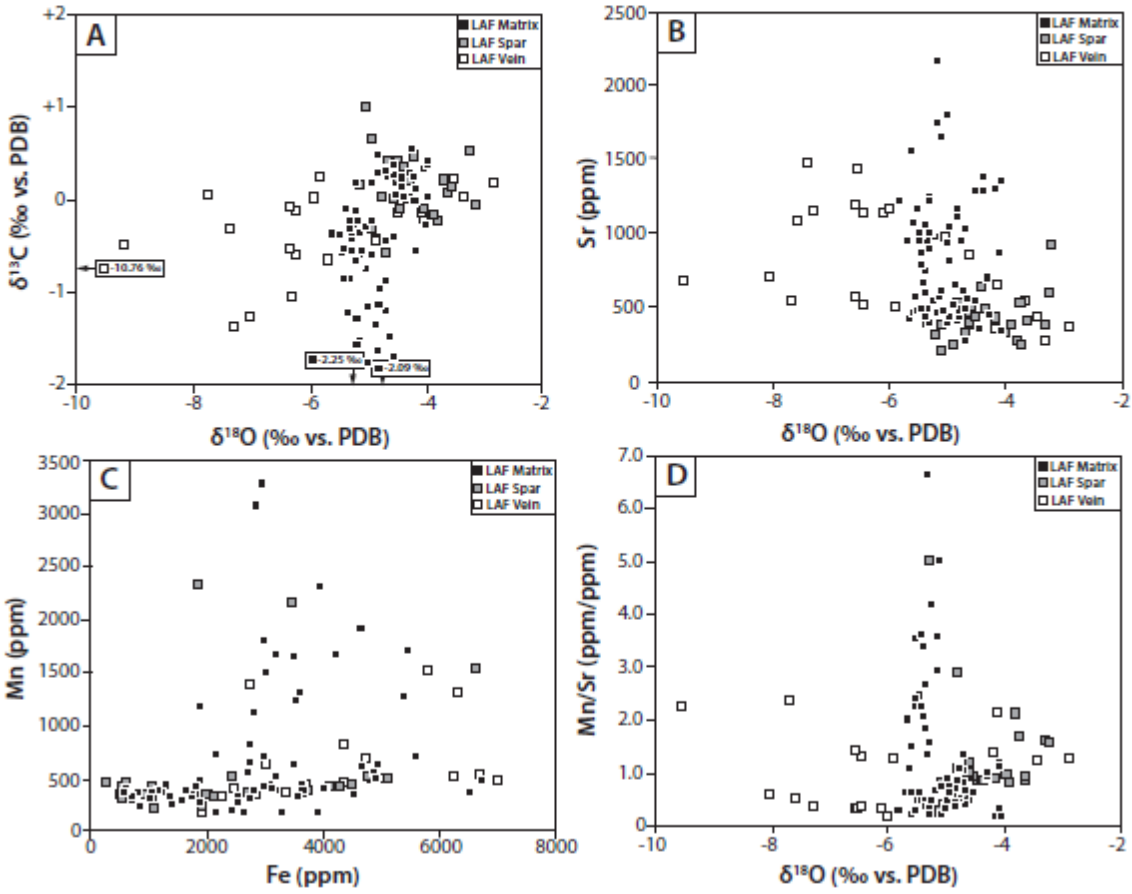

Figure 10

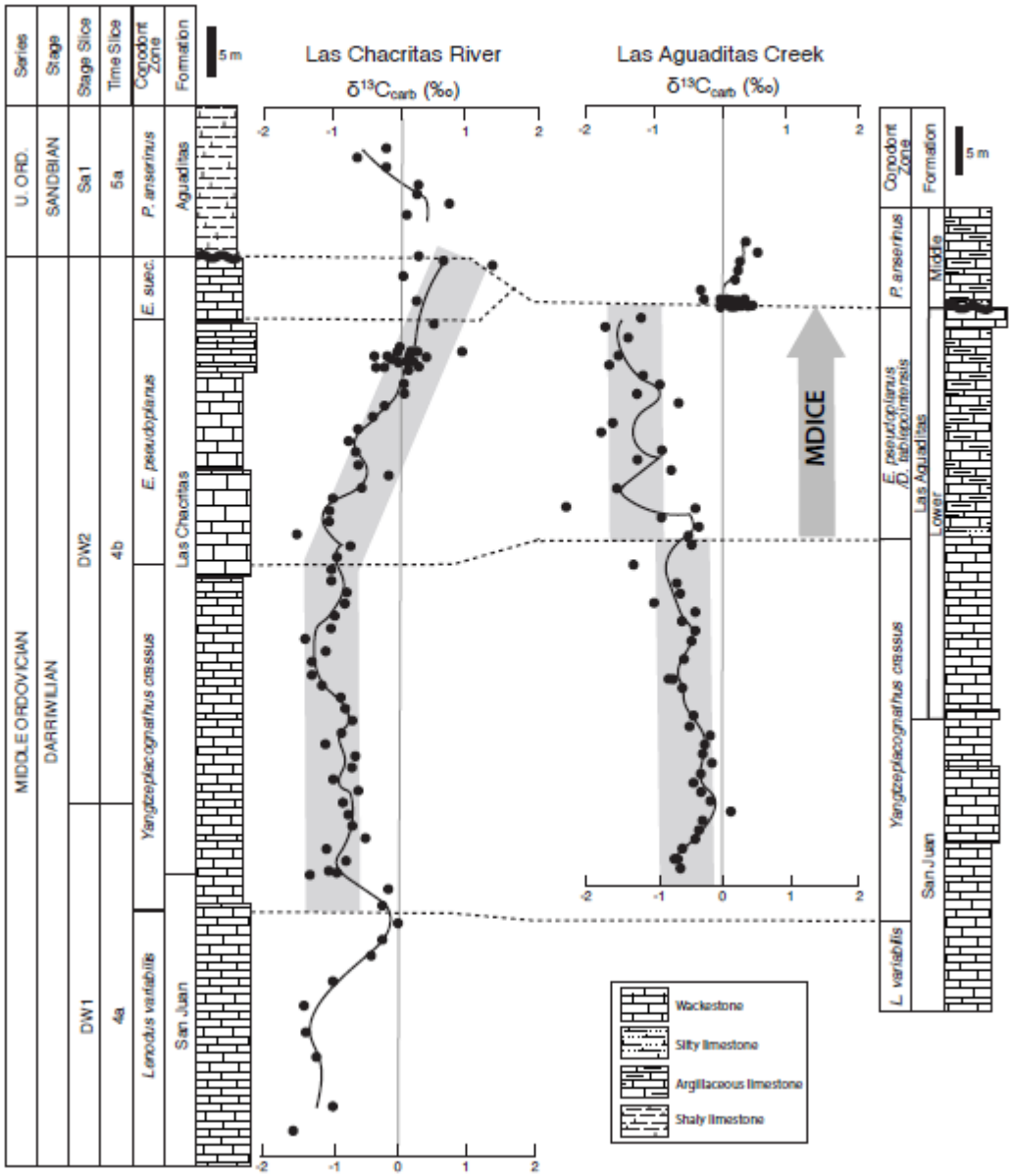

Figure 11

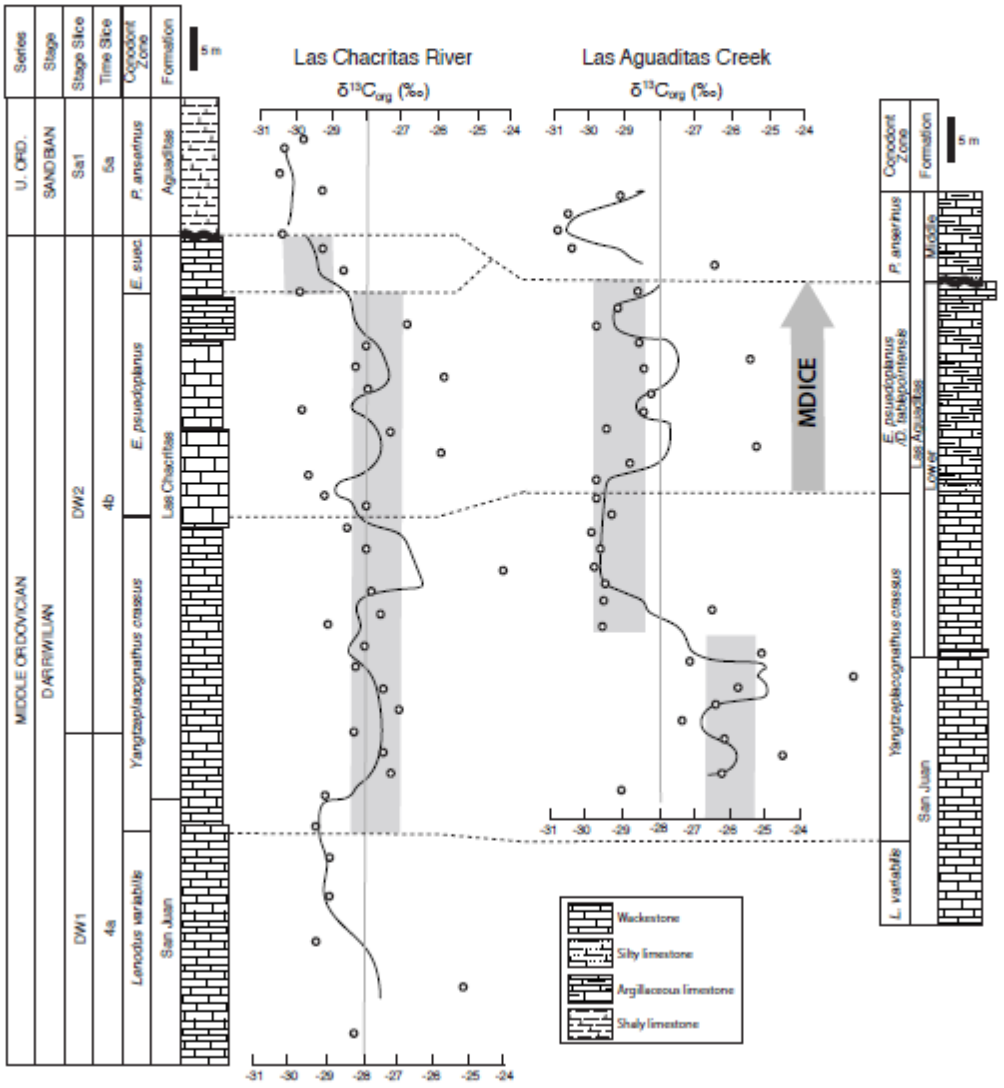

Figure 12

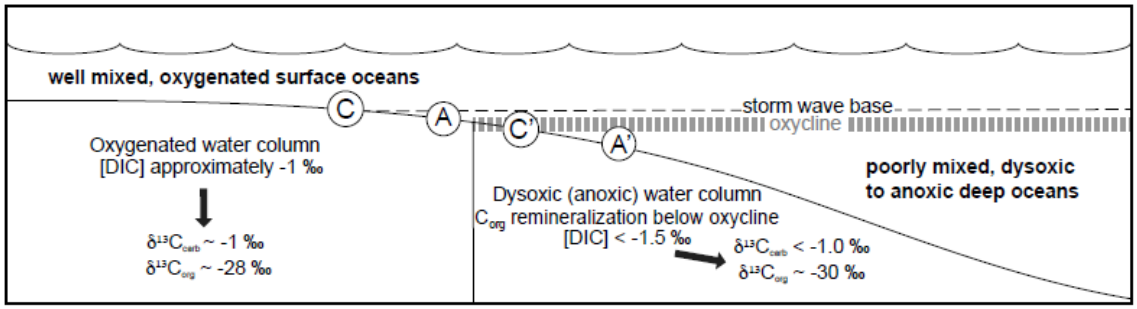

Table 1

Range of isotopic compositions and elemental concentrations recorded in the Las Chacritas Formation

Sample	Height * (m)	Conodont Zone	Phase	$\delta^{13}C_{carb}$	$\delta^{18}O$	$\delta^{13}C_{org}$	$\Delta^{13}C$	Mg/Ca	Sr (ppm)	Mn	Fe
					(□ PDB)						
C14-1	-27.6	*L. variabilis*	Micrite	-1.48	-5.34	-28.35	26.87	0.02	332	98	421
C14-1	-27.6	*L. variabilis*	Vein	-1.45	-7.02	--	--	0.01	348	101	659
C14-2	-24.9	*L. variabilis*	Micrite	-0.92	-5.50	--	--	0.02	343	393	191
C14-4	-19.6	*L. variabilis*	Micrite	-1.16	-5.40	--	--	0.01	310	269	864
C14-5	-17	*L. variabilis*	Micrite	-1.29	-5.43	-29.44	28.15	0.01	338	304	117
C14-6	-14.3	*L. variabilis*	Micrite	-1.33	-5.61	--	--	0.02	344	380	112
C14-7	-11.7	*L. variabilis*	Micrite	-0.92	-5.42	-29.02	28.10	0.02	325	364	149
C14-8	-9	*L. variabilis*	Micrite	-0.36	-5.51	--	--	0.02	311	893	336
C14-9	-7.2	*L. variabilis*	Micrite	-0.20	-5.63	-29.04	28.84	0.02	319	820	303
C14-10	-5.4	*L. variabilis*	Micrite	0.02	-5.66	--	--	0.02	280	881	253
C14-11	-3.6	*Y. crassus*	Micrite	-0.20	-5.83	-29.42	29.22	0.03	300	527	173
C14-11	-3.6	*Y. crassus*	Vein	-0.20	-7.54	--	--	0.02	885	526	192
C14-12	-1.8	*Y. crassus*	Micrite	-0.11	-5.59	--	--	0.01	350	153	340
C14-13	-0.2	*Y. crassus*	Micrite	-1.25	-5.98	-29.14	27.89	0.07	616	806	736
C14-14	0	*Y. crassus*	Micrite	-0.88	-5.77	--	--	0.03	592	719	185
C14-15	1.2	*Y. crassus*	Micrite	-0.97	-5.69	-29.16	28.19	0.01	507	735	105
C14-16	2.3	*Y. crassus*	Micrite	-0.76	-5.86	--	--	0.02	575	673	264
C14-17	3.5	*Y. crassus*	Micrite	-1.03	-5.95	-27.34	26.31	0.03	721	502	183
C14-	3.5	*Y. crassus*	Vein	-0.60	-7.38	--	--	0.00	425	522	150

17								2	9	2	2
C14-			Micrit					0.0	49	34	140
18	4.7	*Y. crassus*	e	-0.45	-5.84	--	--	3	6	0	0
C14-								0.0	65	37	167
18	4.7	*Y. crassus*	Vein	-0.98	-5.59	--	--	2	4	4	3
C14-			Micrit			-		0.0	49	35	143
19	5.9	*Y. crassus*	e	-0.63	-5.97	27.53	26.90	4	9	7	8
C14-			Micrit					0.0	68	33	126
20	7	*Y. crassus*	e	-0.69	-5.69	--	--	1	1	6	6
C14-								0.0	65	36	103
20	7	*Y. crassus*	Vein	-0.81	-5.29	--	--	1	6	3	7
C14-			Micrit			-		0.0	67	39	238
21	8.2	*Y. crassus*	e	-0.78	-5.51	28.34	27.56	2	1	2	2
C14-			Micrit					0.0	65	35	238
22	9.4	*Y. crassus*	e	-0.56	-6.15	--	--	2	3	8	8
C14-			Micrit			-		0.0	73	34	651
23a	11.7	*Y. crassus*	e	-0.92	-5.87	27.10	26.18	0	5	6	2
C14-			Micrit					0.0	67	41	192
23b	11.7	*Y. crassus*	e	-0.91	-5.58	--	--	0	2	1	0
C14-								0.0	51	40	180
23	11.7	*Y. crassus*	Vein	-0.82	-7.20	--	--	0	3	4	3
C14-			Micrit					0.0	73	33	191
24	11.2	*Y. crassus*	e	-0.64	-5.92	--	--	3	0	3	4
C14-			Micrit			-		0.0	94	65	623
25	12.4	*Y. crassus*	e	-0.60	-5.74	27.54	26.94	1	6	3	3
C14-			Micrit					0.0	67	40	148
26	13.6	*Y. crassus*	e	-1.03	-5.99	--	--	0	0	3	7
C14-			Micrit			-		0.0	65	29	131
27	14.9	*Y. crassus*	e	-0.79	-5.83	28.29	27.50	1	1	9	6
C14-								0.0	40	35	
27	14.9	*Y. crassus*	Vein	-1.15	-4.53	--	--	0	3	5	839
C14-			Micrit					0.0	59	22	
28	16.1	*Y. crassus*	e	-0.64	-5.84	--	--	1	5	1	675
C14-			Micrit			-		0.0	66	24	359
29	17.4	*Y. crassus*	e	-0.76	-5.80	28.05	27.29	0	2	8	6
C14-			Micrit					0.0	88	29	143
30	18.6	*Y. crassus*	e	-0.81	-5.70	--	--	0	5	8	8
C14-								0.0	58	21	160
30	18.6	*Y. crassus*	Spar	-0.85	-3.02	--	--	0	5	3	2
C14-			Micrit			-		0.0	64	29	480
31	19.8	*Y. crassus*	e	-1.09	-6.21	29.06	27.97	1	8	2	5
C14-			Micrit			-		0.0	81	35	
33	21.1	*Y. crassus*	e	-1.22	-5.94	27.61	26.39	0	9	7	960
C14-	22.3	*Y. crassus*	Micrit	-1.21	-5.72	--	--	0.0	52	41	972

34			e					1	6	6	
C14-35	23.6	*Y. crassus*	Micrite	-1.01	-6.23	-27.87	26.86	0.01	592	403	3629
C14-36	24.8	*Y. crassus*	Micrite	-1.32	-5.79	--	--	0.00	724	297	7674
C14-36	24.8	*Y. crassus*	Vein	-1.17	-4.71	--	--	0.00	204	338	4274
C14-37	26	*Y. crassus*	Micrite	-0.94	-6.06	-24.16	23.22	0.00	544	272	7662
C14-38	27.3	*Y. crassus*	Micrite	-0.89	-6.11	--	--	0.00	612	402	2304
C14-38	27.3	*Y. crassus*	Spar	-1.10	-4.67	--	--	0.00	542	332	7722
C14-39	28.5	*Y. crassus*	Micrite	-0.76	-5.60	-28.00	27.24	0.00	517	363	8563
C14-39	28.5	*Y. crassus*	Spar	-0.94	-5.43	--	--	0.00	489	474	1757
C14-39	28.5	*Y. crassus*	Vein	-0.77	-6.58	--	--	0.00	510	340	1083
C14-40	29.8	*Y. crassus*	Micrite	-0.73	-6.29	--	--	0.00	474	412	1272
C14-40	29.8	*Y. crassus*	Vein	-1.18	-6.35	--	--	0.00	767	383	1424
C14-41	31	*Y. crassus*	Micrite	-0.95	-5.85	-28.54	27.59	0.01	597	435	1679
C14-42	32.3	*Y. crassus*	Micrite	-0.93	-5.78	--	--	0.00	451	412	9372
C14-43	33.5	*Y. crassus*	Micrite	-0.86	-5.51	-28.03	27.17	0.00	452	359	1512
C14-43	33.5	*Y. crassus*	Spar	-0.68	-5.19	--	--	0.00	324	396	1182
C14-43	33.5	*Y. crassus*	Vein	-0.93	-6.85	--	--	0.00	514	409	1967
C14-44	34.7	*Y. crassus*	Micrite	-0.66	-6.28	-29.15	28.49	0.01	402	363	1026
C14-44	34.7	*Y. crassus*	Vein	-0.91	-6.49	--	--	0.01	427	359	1399
C14-45	37.2	*Y. crassus*	Micrite	-0.98	-5.45	-29.61	28.63	0.01	466	466	1479
C14-46	38.5	*Y. crassus*	Micrite	-0.96	-5.93	--	--	0.02	860	506	6236
C14-47	39.7	*Y. crassus*	Micrite	-0.92	-5.98	-25.93	25.01	0.01	576	356	4366
C14-	40.9	*Y. crassus*	Micrit	-0.50	-5.81	--	--	0.0	32	42	141

48			e					1	4	3	4
C14-49	42.2	*Y. crassus*	Micrite	-0.12	-5.70	27.31	27.19	0.01	293	434	1280
C14-50	43.4	*Y. crassus*	Micrite	-0.54	-5.99	--	--	0.01	341	591	1369
C14-51	44.7	*E. psuedoplanus*	Micrite	-0.58	-5.74	29.79	29.21	0.01	450	391	3678
C14-51	44.7	*E. psuedoplanus*	Spar	-0.95	-4.94	--	--	0.00	318	509	632
C14-52	45.9	*E. psuedoplanus*	Micrite	-0.69	-6.35	--	--	0.01	556	631	3956
C14-52	45.9	*E. psuedoplanus*	Vein	-0.44	-7.17	--	--	0.02	1139	304	2301
C14-53	47.1	*E. psuedoplanus*	Micrite	-0.56	-6.26	27.96	27.40	0.02	327	374	659
C14-54	48.4	*E. psuedoplanus*	Micrite	-0.32	-5.78	25.83	25.51	0.01	371	573	2125
C14-55	49.6	*E. psuedoplanus*	Micrite	-0.17	-6.18	28.30	28.13	0.01	352	539	2035
C14-55	49.6	*E. psuedoplanus*	Vein	-0.34	-6.03	--	--	0.01	394	603	3744
C14-56	50.9	*E. psuedoplanus*	Micrite	0.11	-6.18	--	--	0.01	310	608	2735
C14-56	50.9	*E. psuedoplanus*	Spar	-0.01	-6.35	--	--	0.01	342	710	2497
C14-57	52.1	*E. psuedoplanus*	Micrite	0.11	-6.38	28.01	28.12	0.01	352	517	1810
C14-58	53.3	*E. psuedoplanus*	Micrite	0.17	-5.77	--	--	0.01	310	463	1687
C14-78	53.7	*E. psuedoplanus*	Vein	0.27	-5.16	--	--	0.00	496	518	1888

C14-80	53.7	*E. psuedoplanus*	Spar	0.29	-5.11	--	--	0.00	379	457	751
C14-82	53.7	*E. psuedoplanus*	Spar	0.04	-4.38	--	--	0.00	287	673	1335
C14-85	54.1	*E. psuedoplanus*	Spar	0.16	-4.67	--	--	0.00	190	615	969
C14-86	54.1	*E. psuedoplanus*	Spar	0.17	-5.05	--	--	0.00	475	489	3854
C14-58	54.6	*E. psuedoplanus*	Vein	0.03	-6.03	--	--	0.03	1383	172	2459
C14-59	54.6	*E. psuedoplanus*	Micrite	0.18	-5.99	-26.83	27.01	0.01	337	439	1428
C14-59	54.6	*E. psuedoplanus*	Spar	0.29	-5.36	--	--	0.01	319	335	757
C14-90	54.5	*E. psuedoplanus*	Spar	0.07	-3.50	--	--	0.00	416	473	1011
C14-91	54.5	*E. psuedoplanus*	Vein	-0.29	-5.32	--	--	0.00	358	484	1734
C14-92	54.5	*E. psuedoplanus*	Spar	0.15	-5.09	--	--	0.00	409	433	746
C14-94	54.5	*E. psuedoplanus*	Spar	0.25	-5.00	--	--	0.00	298	588	1752
C14-95	54.5	*E. psuedoplanus*	Spar	-0.03	-5.26	--	--	0.00	438	524	1950
C14-96	54.9	*E. psuedoplanus*	Spar	-0.11	-6.94	--	--	0.00	320	773	2008
C14-97	54.9	*E. psuedoplanus*	Spar	0.28	-5.46	--	--	0.00	268	674	988
C14-96	54.9	*E. psuedopl*	Vein	-0.60	-4.99	--	--	0.00	272	548	1577

		anus									
C14-99	54.9	*E. psuedoplanus*	Spar	0.44	-5.24	--	--	0.00	282	743	1687
C14-99	55.3	*E. psuedoplanus*	Vein	0.01	-8.18	--	--	0.00	696	687	2458
C14-100	54.9	*E. psuedoplanus*	Spar	-0.12	-4.92	--	--	0.00	289	713	1215
C14-60	55.8	*E. psuedoplanus*	Micrite	0.07	-5.72	--	--	0.01	436	410	2158
C14-60	55.8	*E. psuedoplanus*	Spar	0.38	-5.09	--	--	0.01	285	306	492
C14-62	58.3	*E. psuedoplanus*	Micrite	0.55	-7.13	-29.87	30.42	0.01	400	278	1405
C14-62	58.3	*E. psuedoplanus*	Vein	0.48	-6.01	--	--	0.01	289	253	658
C14-64	60.8	*E. suecicus*	Micrite	0.30	-5.81	-28.65	28.95	0.01	1000	171	626
C14-65	62	*E. suecicus*	Micrite	--	--	--	--	0.01	1330	286	1081
C14-66	63.3	*E. suecicus*	Micrite	0.10	-6.39	-29.23	29.33	0.01	762	233	889
C14-66	63.3	*E. suecicus*	Vein	0.02	-8.80	--	--	0.01	872	282	2152
C14-67	64.5	*E. suecicus*	Micrite	1.41	-7.23	--	--	0.01	621	169	767
C14-67	64.5	*E. suecicus*	Vein	0.64	-8.12	--	--	0.01	553	123	464
C14-68	65	*E. suecicus*	Micrite	0.70	-6.94	-30.32	31.02	0.01	695	203	1421
C14-68	65	*E. suecicus*	Vein	0.69	-7.20	--	--	0.01	733	262	1832
C14-69	65.5	*E. suecicus*	Micrite	0.33	-6.84	--	--	0.01	1075	534	8362
C14-70	70	*E. suecicus*	Micrite	0.18	-6.76	-29.22	29.40	0.02	854	446	6954
C14-71	71	*E. suecicus*	Micrite	0.78	-7.01	--	--	0.01	1021	472	5115

C14-72	72	*P. anserinus*	Micrite	0.30	-6.79	-30.45	-30.75	0.03	10 53	60 2	114 96
C14-73	73	*P. anserinus*	Micrite	0.33	-6.98	--	--	0.01	10 78	43 8	587 6
C14-74	74	*P. anserinus*	Micrite	-0.14	-7.03	-30.31	-30.17	0.01	10 66	47 0	639 4
C14-76	76	*P. anserinus*	Micrite	-0.56	-6.44	-29.74	-29.18	0.01	60 3	42 0	244 8
C14-77	77	*P. anserinus*	Micrite	-0.15	-6.73	--	--	0.01	78 5	58 4	361 7

*Height relative to the contact between the San Juan and Las Aguaditas Formations

Table 2

Range of isotopic compositions and elemental concentrations recorded in the Las Aguaditas Formation

Sample	Height* (m)	Conodont Zone	Phase	$\delta^{13}C_{carb}$	$\delta^{18}O$ (‰ PDB)	$\delta^{13}C_{org}$	$\Delta^{13}C$	Mg/Ca	Sr (ppm)	Mn	Fe
A14-1	-16	*Y. crassus*	Micrite	-0.58	-5.62	-29.12	28.54	0.01	431	456	1909
A14-2	-15	*Y. crassus*	Micrite	-0.61	-5.29	--	--	0.01	405	627	2764
A14-2	-15	*Y. crassus*	Micrite	-0.66	-5.36	--	--	0.01	396	716	2194
A14-2	-15	*Y. crassus*	Vein	-0.64	-5.88	--	--	0.02	503	621	3930
A14-3	-14	*Y. crassus*	Micrite	-0.54	-5.58	-26.37	25.83	0.01	474	690	3005
A14-3	-14	*Y. crassus*	Vein	-0.59	-6.44	--	--	0.02	524	671	4736
A14-4	-13	*Y. crassus*	Micrite	-0.36	-5.65	--	--	0.02	409	807	2781
A14-4	-13	*Y. crassus*	Vein	-0.53	-6.56	--	--	0.01	577	804	4362
A14-5	-12	*Y. crassus*	Micrite	-0.29	-5.49	-24.70	24.41	0.02	488	1119	2832
A14-6	-11	*Y. crassus*	Micrite	-0.23	-5.38	--	--	0.01	599	1213	3547
A14-7	-10	*Y. crassus*	Micrite	0.19	-5.36	-26.30	26.49	0.02	443	1118	1890
A14-7	-10	*Y. crassus*	Vein	-0.32	-7.67	--	--	0.02	551	1294	1963
A14-8	-9	*Y. crassus*	Micrite	-0.12	-5.43	--	--	0.01	501	1795	3009
A14-9	-8	*Y. crassus*	Micrite	-0.26	-5.14	-27.46	27.20	0.01	466	1658	4227
A14-10	-7	*Y. crassus*	Micrite	-0.37	-5.41	--	--	0.03	675	1490	3434
A14-	-7	*Y. crassus*	Vein	-0.21	-4.13	--	--	0.0	65	13	27

10								2	1	69	70
A14-11	-6	*Y. crassus*	Micrite	-0.28	-5.23	-26.54	-26.26	0.01	550	2297	3964
A14-12	-5	*Y. crassus*	Micrite	-0.10	-5.54	--	--	0.03	578	1300	3632
A14-12	-5	*Y. crassus*	Vein	-0.48	-9.54	--	--	0.01	686	1512	5821
A14-13	-4	*Y. crassus*	Micrite	-0.25	-5.13	-25.90	-25.65	0.03	572	1654	3225
A14-14	-3	*Y. crassus*	Micrite	-0.22	-5.10	--	--	0.02	614	3065	2865
A14-15	-2	*Y. crassus*	Micrite	-0.13	-5.37	-22.76	-22.63	0.01	487	1644	3521
A14-16	-1	*Y. crassus*	Micrite	-0.43	-5.44	-27.25	-26.82	0.01	783	1897	4662
A14-16	-1	*Y. crassus*	Spar	-0.31	-5.44	--	--	0.02	956	2156	3498
A14-17	0	*Y. crassus*	Micrite	-0.37	-5.32	-25.27	-24.90	0.01	492	3274	2963
A14-17	0	*Y. crassus*	Spar	0.18	-5.28	--		0.02	462	2318	7474
A14-20	3	*Y. crassus*	Micrite	-0.55	-4.30	-29.61	-29.06	0.05	705	6953	5606
A14-21	4	*Y. crassus*	Micrite	-0.69	-5.32	--	--	0.03	963	1254	5403
A14-21	4	*Y. crassus*	Micrite	-0.73	-5.19	--	--	0.04	975	6155	4959
A14-22	5	*Y. crassus*	Micrite	--	--	-26.63	--	--	--	--	--
A14-23	6	*Y. crassus*	Micrite	-0.52	-5.58	-29.58	-29.06	0.03	1075	6223	3523
A14-25	8	*Y. crassus*	Micrite	-0.41	-4.69	-29.55	-29.14	0.02	857	3790	3081
A14-26	9	*Y. crassus*	Micrite	-0.36	-5.28	--	--	0.01	1010	3800	3535

A14-26	9	*Y. crassus*	Vein	-0.43	-5.03	--	--	0.02	979	326	2857
A14-27	10	*Y. crassus*	Micrite	-0.54	-5.44	-29.86	-29.32	0.03	991	587	4670
A14-28	11	*Y. crassus*	Micrite	-0.36	-5.28	--	--	0.01	906	378	2814
A14-29	12	*Y. crassus*	Micrite	-0.95	-4.95	-29.71	-28.76	0.04	815	484	4902
A14-30	13	*Y. crassus*	Micrite	-0.57	-5.27	--	--	0.03	1016	396	4069
A14-31	14	*Y. crassus*	Micrite	-0.63	-5.28	-29.92	-29.29	0.03	1250	317	1764
A14-33	16	*Y. crassus*	Micrite	-1.28	-5.36	-29.38	-28.10	0.03	1060	427	3670
A14-35	18	*Y. crassus*	Micrite	-0.40	-5.69	-29.79	-29.39	0.00	951	540	4880
A14-36	19	*E. psuedoplanus/D. tablepointensis*	Micrite	-0.45	-4.85	--	--	0.02	663	302	2767
A14-37	20	*E. psuedoplanus/D. tablepointensis*	Micrite	-0.29	-5.48	-29.79	-29.50	0.02	959	413	2626
A14-38	21	*E. psuedoplanus/D. tablepointensis*	Micrite	-0.84	-5.48	--	--	0.01	1011	391	2422
A14-39	22	*E. psuedoplanus/D. tablepointensis*	Micrite	-0.36	-5.81	-28.89	-28.53	0.01	1229	267	1069
A14-39	22	*E. psuedoplanus/D. tablepointensis*	Spar	1.00	-5.19	--	--	0.01	994	206	1115
A14-40	23	*E. psuedoplanus/D. tablepointensis*	Micrite	-2.25	-5.42	--	--	0.01	866	369	1643
A14-40	23	*E. psuedoplanus/D. tablepointensis*	Vein	-1.04	-6.52	--	--	0.01	1434	402	3056
A14-41	24	*E. psuedoplanus/D. tablepointensis*	Micrite	-1.52	-5.32	-25.41	-23.89	--	--	--	--
A14-43	26	*E. psuedoplanus/D. tablepointensis*	Micrite	-0.71	-5.29	-29.52	-28.81	0.02	1233	215	873
A14-	27	*E. psuedoplanus/D.*	Micrit	-1.21	-5.51	--	--	0.0	11	28	10

44		*tablepointensis*	e					2	75	2	46
A14-45	28	*E. psuedoplanus/D. tablepointensis*	Micrite	-0.84	-5.60	-28.51	-27.67	0.01	15 60	28 0	16 09
A14-47	30	*E. psuedoplanus/D. tablepointensis*	Micrite	-1.75	-5.15	-28.31	-26.56	0.06	17 48	32 1	35 93
A14-48	31	*E. psuedoplanus/D. tablepointensis*	Micrite	-1.56	-5.36	--	--	0.01	74 3	23 3	14 29
A14-50	33	*E. psuedoplanus/D. tablepointensis*	Micrite	-0.59	-5.08	-28.49	-27.90	0.04	16 52	26 3	25 64
A14-51	34	*E. psuedoplanus/D. tablepointensis*	Micrite	-1.20	-4.83	-25.58	-24.38	0.02	11 20	53 8	27 40
A14-52	35	*E. psuedoplanus/D. tablepointensis*	Micrite	-0.88	-4.82	--	--	0.02	11 56	36 8	18 02
A14-53	36	*E. psuedoplanus/D. tablepointensis*	Micrite	-1.14	-4.96	-28.63	-27.49	0.01	10 48	37 2	11 72
A14-54	37	*E. psuedoplanus/D. tablepointensis*	Micrite	-1.64	-4.98	--	--	0.02	94 4	40 8	10 80
A14-55	38	*E. psuedoplanus/D. tablepointensis*	Micrite	-1.48	-4.76	-29.79	-28.31	0.02	95 5	41 7	13 40
A14-57	40	*E. psuedoplanus/D. tablepointensis*	Micrite	-1.36	-5.00	-29.21	-27.85	0.02	17 95	49 5	32 26
A14-57	40	*E. psuedoplanus/D. tablepointensis*	Vein	-1.37	-7.57	--	--	0.02	10 86	50 0	62 36
A14-58	41	*E. psuedoplanus/D. tablepointensis*	Micrite	-1.69	-4.68	--	--	0.02	10 37	35 7	17 92
A14-58	41	*E. psuedoplanus/D. tablepointensis*	Vein	-1.26	-7.28	--	--	0.01	11 57	35 6	36 64
A14-59	42	*E. psuedoplanus/D. tablepointensis*	Micrite	-1.16	-5.17	--	--	0.03	21 66	47 5	67 15
A14-59	42	*E. psuedoplanus/D. tablepointensis*	Micrite	-2.09	-4.88	-28.68	-26.59	0.02	51 8	29 0	10 21
A14-65	43.2	*P. anserinus*	Micrite	0.42	-4.07	--	--	0.01	35 2	37 8	62 5
A14-66	44.2	*P. anserinus*	Spar	-0.06	-3.22	--	--	0.01	31 9	49 2	24 52
A14-	43.2	*P. anserinus*	Spar	0.48	-4.33	--	--	0.0	60	48	51

77								0	0	2	32
A14-								0.0	85	41	37
77	43.2	*P. anserinus*	Vein	-0.13	-4.62	--	--	0	9	1	28
A14-								0.0	92	21	19
82	43.2	*P. anserinus*	Spar	-0.31	-5.09	--	--	0	4	2	42
A14-								0.0	49	32	21
87	43.2	*P. anserinus*	Spar	0.03	-4.90	--	--	0	3	0	65
A14-								0.0	71	38	24
87	43.2	*P. anserinus*	Vein	0.07	-8.04	--	--	0	3	4	82
A14-								0.0	20	43	62
92	43.2	*P. anserinus*	Spar	0.22	-3.80	--	--	0	7	2	8
A14-			Micro					0.0	32	37	65
64	43.4	*P. anserinus*	spar	0.03	-4.07	--	--	2	7	4	9
A14-								0.0	24	40	57
64	43.4	*P. anserinus*	Spar	0.07	-3.73	--	--	1	7	8	8
A14-								0.0	27	43	27
64	43.4	*P. anserinus*	Vein	0.52	-3.30	--	--	1	8	6	8
A14-								0.0	38	33	52
78	43.4	*P. anserinus*	Spar	0.36	-4.50	--	--	0	0	2	8
A14-								0.0	36	48	48
78	43.4	*P. anserinus*	Vein	-0.13	-4.18	--	--	0	2	2	31
A14-								0.0	53	41	43
83	43.4	*P. anserinus*	Spar	-0.23	-3.90	--	--	0	5	4	08
A14-								0.0	43	51	66
83	43.4	*P. anserinus*	Vein	0.03	-3.43	--	--	0	4	9	81
A14-								0.0	43	51	48
88	43.4	*P. anserinus*	Spar	-0.09	-4.59	--	--	0	9	0	02
A14-								0.0	11	34	33
88	43.4	*P. anserinus*	Vein	-0.10	-6.44	--	--	0	44	6	67
A14-								0.0	38	29	59
93	43.4	*P. anserinus*	Spar	0.66	-5.08	--	--	0	8	1	1
A14-								0.0	46	44	43
93	43.4	*P. anserinus*	Vein	0.20	-4.60	--	--	0	8	4	81
A14-								0.0	24	40	57
65	44.4	*P. anserinus*	Spar	0.07	-3.73	--	--	1	7	8	8
A14-								0.0	51	41	41
79	43.6	*P. anserinus*	Spar	0.15	-3.64	--	--	0	2	7	25
A14-								0.0	38	32	96
84	43.6	*P. anserinus*	Spar	-0.09	-4.16	--	--	0	7	6	9
A14-								0.0	41	32	20
89	43.6	*P. anserinus*	Spar	0.34	-4.77	--	--	0	9	1	35
A14-								0.0	54	47	50
89	43.6	*P. anserinus*	Vein	0.25	-3.63	--	--	0	8	8	14
A14-	43.8	*P. anserinus*	Micrit	0.25	-4.80	--	--	0.0	49	29	11

62			e					1	6	8	25
A14-								0.0	11	30	23
62	43.8	*P. anserinus*	Vein	0.03	-6.11	--	--	2	39	4	01
A14-								0.0	43	34	18
80	43.8	*P. anserinus*	Spar	0.20	-4.39	--	--	0	1	2	24
A14-								0.0	45	41	44
85	43.8	*P. anserinus*	Spar	-0.17	-3.97	--	--	0	3	8	99
A14-								0.0	64	35	27
90	43.8	*P. anserinus*	Spar	0.01	-4.69	--	--	0	0	6	11
A14-								0.0	11	31	20
90	43.8	*P. anserinus*	Vein	-0.07	-6.56	--	--	0	89	8	26
A14-			Micrit					0.0	45	39	36
61	44	*P. anserinus*	e	0.11	-4.28	--	--	1	0	1	78
A14-								0.0	33	32	54
61	44	*P. anserinus*	Spar	0.43	-4.62	--	--	1	7	5	8
A14-								0.0	38	34	17
81	44	*P. anserinus*	Spar	0.23	-4.62	--	--	0	8	8	00
A14-								0.0	37	46	69
81	44	*P. anserinus*	Vein	0.20	-2.88	--	--	0	6	5	92
A14-								0.0	46	36	37
86	44	*P. anserinus*	Spar	0.01	-4.45	--	--	0	1	9	78
A14-								0.0	53	15	66
91	44	*P. anserinus*	Spar	-0.58	-4.82	--	--	0	0	19	44
						-					
A14-			Micrit			26.	26.	0.0	88	24	19
66	45	*P. anserinus*	e	-0.26	-4.10	57	31	3	0	4	08
A14-			Micrit					0.0	12	16	39
67	46	*P. anserinus*	e	0.24	-4.51	--	--	1	95	4	38
						-					
A14-			Micrit			30.	30.	0.0	12	16	33
68	47	*P. anserinus*	e	0.29	-4.39	47	76	1	88	4	00
A14-								0.0	11	15	19
68	47	*P. anserinus*	Vein	0.24	-6.00	--	--	1	73	6	33
A14-			Micrit					0.0	13	16	21
69	48	*P. anserinus*	e	0.33	-4.15	--	--	1	09	3	97
						-					
A14-			Micrit			30.	31.	0.0	13	17	24
70	49	*P. anserinus*	e	0.56	-4.37	84	40	3	83	2	59
A14-			Micrit					0.0	13	17	26
71	50	*P. anserinus*	e	0.39	-4.06	--	--	3	65	1	59
						-					
A14-			Micrit			30.					
72	51	*P. anserinus*	e	--	--	59	--	--	--	--	--
A14-	53	*P. anserinus*	Micrit	--	--	-	--	--	--	--	--

74			e			29.14-						
A14-76	55	*P. anserinus*	Micrite	--	--	26.64	--	--	--	--	--	

*Height relative to the contact beteen the San Juan and Las Aguaditas Formations

Table 3
Summary of Darriwilian isotopic and elemental compositions from the Precordillera

		$\delta^{13}C_{carb}$	$\delta^{18}O$ (‰ PDB)	$\delta^{13}C_{org}$	Sr	Mn (ppm)	Fe
Las Chacritas River Section							
Matrix							
	Average	-0.39	-5.74	-28.32	53	47	25
	St. Dev.	0.59	0.74	1.37	25	19	18
Spar							
	Average	-0.11	-5.03	--	36	52	13
	St. Dev.	0.48	0.81	--	3	1	98
Veins							
	Average	-0.46	-6.46	--	58	37	16
	St. Dev.	0.60	1.14	--	7	9	09
L. variabilis							
	Average	-0.85	-5.50	-28.23	32	48	17
	St. Dev.	0.51	0.11	1.50	19	8	7
Y. crassus							
	Average	-0.82	-5.86	-27.96	60	45	22
	St. Dev.	0.29	0.20	1.23	1	9	92
E. psuedoplanus							
	Average	0.04	-5.26	-28.08	33	53	24
	St. Dev.	0.34	0.94	1.35	72	7	5

E. suecicus							
			-6.71	-29.35	92	31	31
	Average	0.54			0	4	52
	St. Dev.	0.43	0.4	0.61	21 8	13 8	29 56
P. anserinus							
			-6.79	-30.16	91 7	50 3	59 66
	Average	-0.04					
	St. Dev.	0.33	0.2 1	0.31	19 1	76	31 20
Las Aguaditas Creek Section							
Matrix							
			-4.98	-28.17	78 8	64 2	26 68
	Average	-0.38					
	St. Dev.	0.65	0.4 7	1.91	40 2	61 8	14 95
Spar							
			-4.39		46 7	54 9	22 64
	Average	0.14		--			
	St. Dev.	0.33	0.6 2	--	19 8	51 9	16 88
Veins							
			-2.88		14 34	15 12	69 92
	Average	0.52		--			
	St. Dev.	0.48	1.92	--	33 3	34 9	17 11
L. variabilis		--	--	--	--	--	--
Y. crassus							
			-5.31	-27.67	70 8	10 95	35 00
	Average	-0.44					
	St. Dev.	0.27	0.2 7	2.08	24 8	76 3	10 08
E. psuedoplanus							
			-5.16	-28.40	11 79	35 3	11 79
	Average	-1.19					
	St. Dev.	0.54	0.3	1.39	40	86	40

		1		4		4
E. suecicus	--	--	--	--	--	--
P. anserinus						
		-	-			
	0.22	4.53	29.04	605	356	2124
Average						
	0.18	0.35	1.81	348	263	1601
St. Dev.						

Highlights:

• Paired carbon isotopes of carbonate and organic matter constrain marine system

• Darriwilian MDICE excursion is coincident with climate and ocean chemistry change

• Las Chacritas and Las Aguaditas formations record facies on deepening marine shelf

• Carbon isotopes show initiation of MDICE excursion in onshore, but not offshore, environments

• Paired isotopes suggest marine chemocline remains apparent through the Darriwilian